Modeling and Fuzzy Decoupling Control of an Underwater Vehicle-Manipulator System

HAN HAN[1], YANHUI WEI[1], XIUFEN YE[1], AND WENZHI LIU[2]

[1]College of Automation, Harbin Engineering University, Harbin 150001, China
[2]College of Information and Communication Engineering, Harbin Engineering University, Harbin 150001, China

Corresponding author: Yanhui Wei (wyhhit@163.com)

ABSTRACT This paper presents the detailed modeling and simulation of the dynamic coupling between an autonomous underwater vehicle (AUV) and a manipulator. The modeling processes are described with the incorporation of the most dominating hydrodynamic effects such as added mass, lift and drag forces. The hydrodynamic coefficients are derived using strip theory and are adjusted according to dynamical similarity. A fuzzy decoupling controller (FDC) is proposed for an autonomous underwater vehicle-manipulator system (UVMS) which consists of two subsystems, an underwater vehicle and a manipulator. The proposed controller uses a fuzzy algorithm (FA) to adaptively tune the gain matrix of the error function (EF). The EF is described by the integral sliding surface function. This technique allows the off-diagonal elements developed for decoupling the system to be incorporated in the gain matrix. Tracing the FA and EF back to the principle of feedback linearization, one further obtains evidence about the decoupling and stability of the system. Moreover, a desired trajectory with the consideration of the dynamic coupling of the AUV is designed to reduce the thruster forces and manipulator's torques. This technique provides high performance in terms of tracking error norms and expended energy norms. A major contribution of this study is that it adopts the off-diagonal elements to exploit the dynamic coupling between the degrees of freedom of the subsystem and the dynamic coupling between the two subsystems. Simulation results demonstrate the effectiveness and robustness of the proposed technique in the presence of parameter uncertainties and external disturbances.

INDEX TERMS AUV, dynamic coupling, decoupling control, fuzzy algorithm, hydrodynamic effect, underwater manipulator.

I. INTRODUCTION

AUVs equipped with on-board manipulators play an increasingly important role in marine research in recent years. Such systems called autonomous underwater vehicle-manipulator systems (UVMSs) are required in many applications, such as performing grabbing, sampling, opening and closing valves. With the wide uses of such systems, there is a concomitant need for accurate simulations. Dynamic simulation can be a beneficial tool in the development of UVMSs. Simulators can aid in the design of control approaches. By testing these approaches on simulators, the possibility of potentially damaging instabilities due to algorithm errors can be eliminated and the risks encountered when the control system is

The associate editor coordinating the review of this manuscript and approving it for publication was Xudong Zhao.

implemented in hardware can be reduced [1]. The interaction between the dynamics of the vehicle and the manipulator is strong due to hydrodynamic forces [2]. Moreover, the effect of hydrodynamics acting on the UVMS is to add the nonlinearities and uncertainties of the dynamics [3]–[6]. In order to achieve precise control of the UVMS, it is crucial to develop a stable, robust and high-performance decoupling control approach based on accurate dynamic simulations. Simultaneously, a proper geometric configuration of the AUV hull is also essential, as it could generate the smallest hydrodynamic forces.

The torpedo-type AUV is widespreadly used by all major manufacturers of AUVs due to its good features that generate the smallest possible drag coefficients [7], [8]. In order to simplify modeling, the hull of AUV is assumed to be a spheroid or a cylinder to calculate the hydrodynamic coefficients [3].

As to the torpedo-type AUV called REMUS, Prestero [9] used the strip integral method which is similar to strip theory [10], [11] to calculate the added mass, drag and lift coefficients. In addition, the author found it necessary to adjust a subset of the calculated coefficients derived using the strip integral method, and these adjustments were based on comparisons with the experimental data [9]. It is discovered that the more accurate nondimensional hydrodynamic coefficients [12] for torpedo-type AUVs can be obtained based on comparisons with those of the REMUS data [9], [13].

After the dynamic model of the UVMS is developed, an appropriate control scheme can be developed. The coupling effects of the UVMS [14]–[16] are to increase the difficulty and complexity of designing appropriate controllers. The control approach to decouple the system based on feedback linearization is most used by researchers. Santhakumar [17] proposed a model reference control scheme for the UVMS. Korkmaz *et al.* [18] presented an inverse dynamics control law for an underactuated UVMS (U-UVMS). Taira et al. [19] developed a model-based control for the UVMS with one of the three types of servo subsystems. These methods are dependent on the detailed dynamic model of the system. However, in practice, it is rather difficult to obtain the exact hydrodynamic parameters in the underwater environment.

To overcome this problem, adaptive control methods have been proposed. Mahesh *et al.* [20] proposed a discrete-time adaptive control strategy for the coordinated control of an underwater vehicle and its robotic manipulator. Antonelli *et al.* [21] proposed a new adaptive control scheme for the tracking problems of the UVMS based on virtual decomposition approach which requires a reduced-order regressor. Taira et al. [22] developed an adaptive controller that uses radius basis function networks instead of feedforward terms including the regressors of dynamic system models. However, larger parameter uncertainties are difficult to adapt in these methods. Santhakumar and Kim [23] presented an indirect adaptive control method for the UVMS based on an extended Kalman filter (EKF); however the performance of this method is highly dependent on the performance of estimation, and the performance can be significantly degraded when the estimation has large errors. Dai and Yu [24] proposed an indirect adaptive control method for the UVMS based on an EKF and a H_∞ controller; however its control performance depends on the prior knowledge of the worst case disturbance assumption.

Therefore, it is necessary to design a robust and no-model-based controller for the UVMS. Sliding mode control (SMC) has been widely used as a robust and nonlinear controller for the UVMS [14], [25], [26]. It maintains high robustness against parameter uncertainties and external disturbances. However, SMC suffers from the chattering phenomenon. To handle this issue, the fuzzy logic control (FLC) is presented to adaptively tune the gains of SMC [27], [28]. Esfahani *et al.* [29] presented an improved Time Delay Controller (TDC) consisting of a TDC term,

a Terminal Sliding Mode (TSM) term and a proportional-integral-derivative (PID) term for the UVMS, and the fuzzy rules were used to adaptively tune the gains of TSM and PID terms. Even though the chattering was significantly reduced, it was not completely eliminated.

Recently, the fusion of FLC with robust control (RC) has become a most promising control technique [30]–[38]. Because fuzzy logic controllers are usually designed based on intuitive standpoint, they are often more understandable [27]. Moreover, the performance and stability of robust fuzzy controllers can be ensured and meanwhile the number of fuzzy rules can be reduced [39]. Londhe presented a robust nonlinear PID-like fuzzy control scheme [40] and a new robust single-input fuzzy logic control scheme [41] for a task-space trajectory tracking control of the UVMS. Although there have been some research attempts to investigate the coupling effects due to hydrodynamic effects in the case of external disturbances, e.g. ocean currents, modelling these is still an open research topic. And very few research attempts to achieve both decoupling between the degrees of freedom of the subsystem and decoupling between the two subsystems. Moreover, when the desired trajectory of the system is designed, it is rarely to take the coupling effects into consideration. In addition to the coupling effects, the AUV used in practical applications is generally not fully actuated which complicates the problem.

Considering the aforementioned issues, this paper presents the closed-form dynamic equation of an UVMS. The UVMS consists of two subsystems, e.g. a torpedo-type AUV and a three-degrees-of-freedom manipulator. The hydrodynamic coefficients of the AUV are derived using strip theory and then are adjusted based on comparisons with the REMUS data [9] in terms of dynamical similarity. The hydrodynamic effects are incorporated in the dynamic equations of the manipulator as well. This paper also proposes a fuzzy decoupling controller (FDC) which is based on the fusion of the fuzzy algorithm (FA), error function (EF) and feedback linearization. The gain matrix of EF tuned by FA includes the off-diagonal elements to decouple the UVMS which has the nature of dynamic coupling. The estimations of the system matrices are incorporated in the controller as well. In addition, a desired decoupling trajectory for the AUV is designed. The key advantage of this method is that it achieves decoupling and linearization of the system, and also it ensures precise and robust performance in the case of parameter uncertainties and external disturbances. Simulation results are presented to demonstrate the superiority of the FDC over both the traditional fuzzy controller (FC) and the conventional PID controller with the inverse dynamic (ID) model as a feedforward control (PIDID). The gain matrix of FC does not incorporate the off-diagonal elements.

The rest of the paper is organized as follows. Section II describes the kinematic and dynamic modelings of the UVMS. The fuzzy decoupling controller is proposed in Section III. Simulation experiments along with comparative
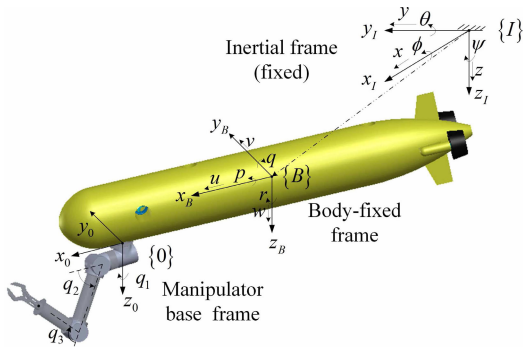
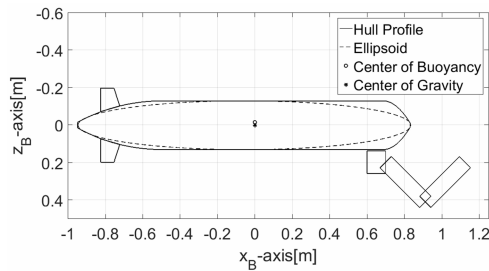**FIGURE 1.** Profile and coordinate systems of the UVMS.

FIGURE 2. Profile of the UVMS in the x_B-z_B plane.

FIGURE 3. Profile of the AUV and geometric parameters of Mying equations.

FIGURE 4. Link coordinate systems of the manipulator.

TABLE 1. D-H parameters of the manipulator.

Joint(k)	offset(α_{k-1})	length (a_{k-1})	distance(d_k)	angle(θ_k)
1	$0°$	0	0	q_1
2	$90°$	l_{q1}	0	q_2
3	$0°$	l_{q2}	0	q_3
4	$0°$	l_{q3}	0	$q_4 = 0°$

studies are conducted in Section IV. Section V holds the conclusions.

II. MODELING

A. KINEMATICS

The profile of the proposed UVMS is shown in Fig.1. The motions of AUV include surge, sway, heave, roll, pitch and yaw. In the Inertial frame $\{I\}$, the position vector is described by the vector $\boldsymbol{\eta}_1 = [x, y, z]^T$ and the orientation vector is represented in terms of $\boldsymbol{\eta}_2 = [\phi, \theta, \psi]^T$. Let us define $\boldsymbol{\eta} = [\boldsymbol{\eta}_1^T, \boldsymbol{\eta}_2^T]^T$ and $\dot{\boldsymbol{\eta}} = [\dot{\boldsymbol{\eta}}_1^T, \dot{\boldsymbol{\eta}}_2^T]^T$ the corresponding time derivative. The AUV attitude in terms of quaternions can be denoted with $\boldsymbol{Q}_2 = \{\boldsymbol{\varepsilon}, \eta\}$. In the Body-fixed frame $\{B\}$, the velocity vector is defined as $\boldsymbol{v} = [\boldsymbol{v}_1^T, \boldsymbol{v}_2^T]^T$, where $\boldsymbol{v}_1 = [u, v, w]^T$ is the linear velocity vector and $\boldsymbol{v}_2 = [p, q, r]^T$ is the angular velocity vector. Let $\boldsymbol{q} = [q_1, q_2 \cdots q_n]^T$ be the vector of joint positions, where n is the number of manipulator's link. The vector $\dot{\boldsymbol{q}}$ is the corresponding time derivative. Let us also define $\boldsymbol{\zeta} = [\boldsymbol{v}_1^T, \boldsymbol{v}_2^T, \dot{\boldsymbol{q}}^T]^T$. The coordinate system of manipulator's base mounted on the AUV hull is described by $\{0\}$. Fig.2 shows the profile of the system in x_B-z_B plane of frame $\{B\}$, where the ellipsoid is plotted for reference.

1) KINEMATICS OF THE AUV

The hull of AUV is chosen as a torpedo type due to its good features [7] shown in Fig.3. The profiles of the bow and stern are modeled based on Myring equations [7]. The equations are as follows:

$$\text{Bow}: R(L) = \frac{1}{2}d \left[1 - \left(\frac{L + a_{\text{offset}} - a}{a} \right)^2 \right]^{\frac{1}{n_v}} \quad (1)$$
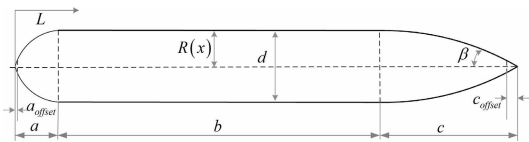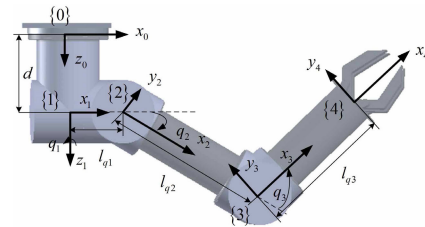
$$\text{Stern}: R(L) = \frac{1}{2}d - \left[\frac{3d}{2c^2} - \frac{\tan\beta}{c} \right](L - l_{\text{f}})^2$$
$$+ \left[\frac{d}{c^3} - \frac{\tan\beta}{c^2} \right](L - l_{\text{f}})^3 \quad (2)$$

where a, b and c are the bow-section length, the midbody-section length and the stern-section length; $l_{\text{f}} = a + b - a_{\text{offset}}$ is the forward body length. a_{offset} and c_{offset} are the missing lengths of the bow and stern respectively; n_v is an exponential parameter of the bow; β is the induced angle at the terminal stern; d is the diameter of the midbody; L is the axial position along the centerline.

The velocity vectors of the AUV which are described in frame $\{B\}$ and frame $\{I\}$ are related via the following relation:

$$\boldsymbol{v} = \boldsymbol{J}(\boldsymbol{\eta})\dot{\boldsymbol{\eta}} \quad (3)$$

where $\boldsymbol{J}(\boldsymbol{\eta}) = \begin{bmatrix} \boldsymbol{R}_I^B & \boldsymbol{0}_{3\times3} \\ \boldsymbol{0}_{3\times3} & \boldsymbol{J}_v \end{bmatrix}$, $\boldsymbol{v}_1 = \boldsymbol{R}_I^B \dot{\boldsymbol{\eta}}_1$, $\boldsymbol{v}_2 = \boldsymbol{J}_v \dot{\boldsymbol{\eta}}_2$. $\boldsymbol{J}(\boldsymbol{\eta})$ is the (6×6) Jacobian matrix of the AUV; $\boldsymbol{R}_I^B$ is the linear velocity transformation matrix and $\boldsymbol{J}_v$ is the angular velocity transformation matrix. The values of $\boldsymbol{R}_I^B$ and $\boldsymbol{J}_v$ both can be expressed in terms of Euler angles (roll (ϕ), pitch (θ) and yaw (ψ)), which can be referred to [21].

Additionally, it is possible to take the effect of the ocean current into consideration, which is described by $\boldsymbol{v}_c$ ($\boldsymbol{v}_c \in \mathbb{R}^{6\times1}$). In the case of an irrotational current, the 4th to 6th elements of $\boldsymbol{v}_c$ are zeros that $\boldsymbol{v}_c = [u_c, v_c, w_c, 0, 0, 0]^T$. Then, the relative velocity is

$$\boldsymbol{v}_r = \boldsymbol{v} - \boldsymbol{J}(\boldsymbol{\eta})\boldsymbol{v}_c \quad (4)$$

2) KINEMATICS OF THE MANIPULATOR

The links of the manipulator are considered as cylinders in shape. Such a shape is one of the primary candidates for the link geometry for underwater manipulators. Fig.4 shows the establishment of the link coordinated systems, which yields D-H parameters shown in Table 1. Based on the parameters of links in Table 1, the homogeneous matrix of manipulator's end-effector with respect to the coordinate system of manipulator's base {0} can be expressed as

$$T_{n+1}^0 = \prod_{k=1}^n T_k^{k-1} = \begin{bmatrix} R_{n+1}^0 & p_{n+1}^0 \\ 0_{3\times1} & 1 \end{bmatrix} \quad (5)$$

where n is the number of manipulator's link. R_{n+1}^0 and p_{n+1}^0 are the rotation matrix and the position vector of frame {$n+1$} relative to frame {0}. T_k^{k-1} is the homogenous matrix of frame {k} relative to frame {$k-1$}.

$$T_k^{k-1} = \begin{bmatrix} R_k^{k-1} & p_k^{k-1} \\ 0_{3\times1} & 1 \end{bmatrix}$$

$$R_k^{k-1} = \begin{bmatrix} \cos q_k & -\sin q_k & 0 \\ \sin q_k \cos\alpha_{k-1} & \cos q_k \cos\alpha_{k-1} & -\sin\alpha_{k-1} \\ \sin q_k \sin\alpha_{k-1} & \cos q_k \sin\alpha_{k-1} & \cos\alpha_{k-1} \end{bmatrix}$$

$$p_k^{k-1} = \begin{bmatrix} a_{k-1} & -\sin\alpha_{k-1} d_k & \cos\alpha_{k-1} d_k \end{bmatrix}^T$$

Therefore, the rotation matrix and the position vector of the manipulator's end-effector with respect to the Body-fixed frame {B} can be represented as

$$R_{n+1}^B = R_0^B R_{n+1}^0 \quad (6)$$
$$p_{n+1}^B = p_0^B + R_0^B p_{n+1}^0 \quad (7)$$

where R_0^B and p_0^B are the rotation matrix and the position vector of frame {0} relative to frame {B}.

B. MOTION EQUATION OF THE SYSTEM

1) DYNAMICS OF THE AUV

The dynamic model of the AUV with the incorporation of the hydrodynamic effects and manipulator disturbances is derived and written in a closed form [3] as

$$M_\nu \dot{\nu} + C_\nu(\nu)\nu + D_\nu(\nu)\nu + g_\nu(\eta) = \tau_\nu + \sigma \quad (8)$$

With the hydrodynamic terms contributed by the velocity ν_r shown in (4), the motion equation of the AUV is

$$M_\nu \dot{\nu}_r + C_\nu(\nu_r)\nu_r + D_\nu(\nu_r)\nu_r + g_\nu(\eta) = \tau_\nu + \sigma_r \quad (9)$$

where

$$M_\nu = M_{RB} + M_A$$
$$C_\nu(\nu_r) = C_{RB}(\nu_r) + C_A(\nu_r)$$
$$D_\nu(\nu_r) = D_{NL}\text{diag}(|\nu_r|) + D_L\text{diag}(|\nu_r|)$$
$$\tau_\nu = BT$$

M_{RB} and C_{RB} are the inertia matrix and the Coriolis and centripetal matrix of the rigid body. M_A and C_A are the added mass matrix and the added Coriolis and centripetal matrix. D_{NL} and D_L are the quadratic damping matrix and
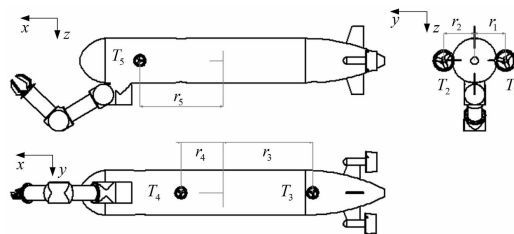

FIGURE 5. Thruster distribution of the AUV.

the lift matrix. $g_\nu(\eta)$ is the vector of gravitational and buoyant forces and moments. τ_ν is the vector of control inputs. $T = [T_1, T_2, T_3, T_4, T_5]^T$ is the vector of thruster forces. $\sigma_r = [\sigma_f^T, \sigma_m^T]^T$ is the disturbance vector of forces and moments due to the manipulator in the presence of ocean currents.

$$M_A = -\begin{bmatrix} X_{\dot{u}} & 0 & 0 & 0 & 0 & 0 \\ 0 & Y_{\dot{v}} & 0 & 0 & 0 & Y_{\dot{r}} \\ 0 & 0 & Z_{\dot{w}} & 0 & Z_{\dot{q}} & 0 \\ 0 & 0 & 0 & K_{\dot{p}} & 0 & 0 \\ 0 & 0 & M_{\dot{w}} & 0 & M_{\dot{q}} & 0 \\ 0 & N_{\dot{v}} & 0 & 0 & 0 & N_{\dot{r}} \end{bmatrix}$$

$$= \begin{bmatrix} A_{11} & A_{12} \\ A_{21} & A_{22} \end{bmatrix}$$

$$C_A = \begin{bmatrix} 0_{3\times3} & -S(A_{11}\nu_1 + A_{12}\nu_2) \\ -S(A_{11}\nu_1 + A_{12}\nu_2) & -S(A_{21}\nu_1 + A_{22}\nu_2) \end{bmatrix}$$

$$D_{NL} = -\begin{bmatrix} X_{u|u|} & 0 & 0 & 0 & 0 & 0 \\ 0 & Y_{v|v|} & 0 & 0 & 0 & Y_{r|r|} \\ 0 & 0 & Z_{w|w|} & 0 & Z_{q|q|} & 0 \\ 0 & 0 & 0 & K_{p|p|} & 0 & 0 \\ 0 & 0 & M_{w|w|} & 0 & M_{q|q|} & 0 \\ 0 & N_{v|v|} & 0 & 0 & 0 & N_{r|r|} \end{bmatrix}$$

$$D_L = -\begin{bmatrix} 0 & 0 & 0 & 0 & 0 & 0 \\ 0 & Y_{uv} & 0 & 0 & 0 & Y_{ur} \\ 0 & 0 & Z_{uw} & 0 & Z_{uq} & 0 \\ 0 & 0 & 0 & 0 & 0 & 0 \\ 0 & 0 & M_{uw} & 0 & M_{uq} & 0 \\ 0 & N_{uv} & 0 & 0 & 0 & N_{ur} \end{bmatrix}$$

$$B = \begin{bmatrix} 1 & 1 & 0 & 0 & 0 \\ 0 & 0 & 0 & 0 & 1 \\ 0 & 0 & 1 & 1 & 0 \\ 0 & 0 & 0 & 0 & 0 \\ 0 & 0 & r_3 & -r_4 & 0 \\ r_1 & -r_2 & 0 & 0 & r_5 \end{bmatrix}$$

where $r = [r_1, r_2, r_3, r_4, r_5]^T$ is the position vector of five thrusters, as shown in Fig.5.

In terms of the shape of the AUV, the above hydrodynamic coefficients in M_A, D_{NL} and D_L have been calculated based on strip theory [9]. Refer to Appendix A for the details. Besides, it is necessary to adjust some coefficients derived in Appendix A. These adjustments are based on comparisons with the nondimensional hydrodynamic coefficients of REMUS [9] in terms of dynamical similarity. The nondimensional factors [12] of hydrodynamic coefficients are shown

TABLE 2. Nondimensional values of AUV coefficients.

Unit	Nondimensional factor $1/(\frac{1}{2}\rho l^3)$			
Kg	$X_{\dot{u}}$	$Y_{\dot{v}}$	$Z_{\dot{w}}$	$M_{w\vert w\vert}$
	$N_{v\vert v\vert}$	M_{uw}	N_{uv}	
Kg/rad	Y_{uv}	Z_{uw}		
Unit	Nondimensional factor $1/(\frac{1}{2}\rho l^4)$			
Kg·m	$Y_{\dot{r}}$	$Z_{\dot{q}}$	$M_{\dot{w}}$	$N_{\dot{v}}$
Kg·m/rad^2	$Y_{r\vert r\vert}$	$Z_{q\vert q\vert}$		
Kg·m/rad	M_{uq}	N_{ur}		
Unit	Nondimensional factor $1/(\frac{1}{2}\rho l^2)$			
Kg/m	$M_{u\vert u\vert}$	$Y_{v\vert v\vert}$	$Z_{w\vert w\vert}$	Y_{uv}
	Z_{uw}			
Unit	Nondimensional factor $1/(\frac{1}{2}\rho l^5)$			
Kg·m^2/rad^2	$K_{\dot{p}}$	$M_{\dot{q}}$	$N_{\dot{r}}$	$K_{p\vert p\vert}$
	$M_{q\vert q\vert}$	$N_{r\vert r\vert}$		

TABLE 3. Adjustment factors of AUV coefficients.

Coefficient	AdjustmentFactor
$K_{p\vert p\vert}$	36
$K_{\dot{p}}$	4.3
$Y_{v\vert v\vert}$	9.7
$M_{q\vert q\vert}$	23
$N_{r\vert r\vert}$	11.6

in Table 2. The adjustment factors list below in Table 3. Note that Table 18 in Appendix A lists the unadjusted hydrodynamic coefficients, while Table 10 in section IV lists the adjusted hydrodynamic coefficients.

2) DYNAMICS OF THE MANIPULATOR

The iterative Newton-Euler formulation is used to derive the dynamic model of the manipulator. Note that the initial velocity of the manipulator is equal to the velocity of the AUV. And the hydrodynamic effects such as: added mass, lift and drag forces are incorporated. The vectors of total forces and moments, $\boldsymbol{F}_k$ and $\boldsymbol{T}_k$, on link k with respect to the link coordinate system $\{k\}$ can be written as

$$\boldsymbol{F}_k = \boldsymbol{M}_k{}^k\dot{\boldsymbol{v}}_{r,k} \tag{10}$$
$$\boldsymbol{T}_k = \boldsymbol{I}_k{}^k\dot{\boldsymbol{\omega}}_k + {}^k\boldsymbol{\omega}_k \times (\boldsymbol{I}_k{}^k\boldsymbol{\omega}_k) \tag{11}$$

where ${}^k\dot{\boldsymbol{v}}_{r,k}$ is the linear acceleration vector of the center of mass of link k with the consideration of the ocean current. In terms of the constant and irrotational ocean current, ${}^k\dot{\boldsymbol{v}}_{r,k} = {}^k\dot{\boldsymbol{v}}_{c,k}$. ${}^k\boldsymbol{\omega}_k$ is the angular velocity of link k, and ${}^k\dot{\boldsymbol{\omega}}_k$ is the corresponding time derivative. Refer to Appendix B for further details of the iterative algorithms. $\boldsymbol{M}_k$ is the mass and added mass matrix of link k. $\boldsymbol{I}_k$ is the matrix of moment of inertia and added moment of inertia of link k.

$$\boldsymbol{M}_k = \begin{bmatrix} m_{qk} + 0.1 m_{qk} & 0 & 0 \\ 0 & m_{qk} + \rho\Delta_k & 0 \\ 0 & 0 & m_{qk} + \rho\Delta_k \end{bmatrix}$$

$$\boldsymbol{I}_k = \begin{bmatrix} I_{x,k} & 0 & 0 \\ 0 & I_{y,k} + \frac{1}{12}\pi\rho r_{qk}^2 l_{qk}^3 & 0 \\ 0 & 0 & I_{z,k} + \frac{1}{12}\pi\rho r_{qk}^2 l_{qk}^3 \end{bmatrix}$$

where m_{qk} is the mass of link k. r_{qk} is the radius of link k. l_{qk} is the length of link k. Δ_k is the displacement volume. ρ is the density of the fluid environment.

The total friction forces and moments acting on the center of mass of link k are

$$\boldsymbol{p}_k = \boldsymbol{F}_L + \boldsymbol{F}_D + \boldsymbol{F}_S \tag{12}$$
$$\boldsymbol{n}_k = \boldsymbol{S}({}^k\boldsymbol{v}_{r,k})[\boldsymbol{M}_k{}^k\boldsymbol{v}_{r,k}] \tag{13}$$

where

$$\boldsymbol{F}_S = \boldsymbol{D}_s{}^k\boldsymbol{v}_{r,k}$$
$$\boldsymbol{F}_D = \frac{1}{2}\rho C_d A_k \mathrm{diag}({}^k\boldsymbol{v}_{r,k}){}^k\boldsymbol{v}_{r,k}$$
$$\boldsymbol{F}_L = \frac{1}{2}\rho C_l A_k \mathrm{diag}({}^k\boldsymbol{v}_{r,k}){}^k\boldsymbol{v}_{r,k}$$

${}^k\boldsymbol{v}_{r,k} = {}^k\boldsymbol{v}_{c,k} - \boldsymbol{R}_I^k[u_c, v_c, w_c]^T$, which is the relative linear velocity of the center of mass of link k with the consideration of the ocean current. $\boldsymbol{v}_{c,k}^k$ is the linear velocity of the center of mass of link k. $[u_c, v_c, w_c]^T$ is the linear velocity of an irrotational current. $\boldsymbol{R}_I^k$ is the rotation matrix of the Inertial frame $\{I\}$ relative to the link coordinate system $\{k\}$. D_s, C_d and C_l are the linear skin-friction coefficient, the drag coefficient and the lift coefficient. A_k is the projected front area of link k. $\boldsymbol{S}$ is a skew-symmetric matrix. And for the cross-product of vectors $\boldsymbol{a}$ and $\boldsymbol{b}$, it has $\boldsymbol{a} \times \boldsymbol{b} = \boldsymbol{S}(\boldsymbol{a})\boldsymbol{b}$.

The buoyancy of link k is

$$\boldsymbol{b}_k = \rho g \Delta_k \tag{14}$$

where g is the gravitational acceleration.

The link is assumed as a negative buoyant body. And the center of buoyancy is coincident with the center of gravity.

The vectors of forces and moments, ${}^k\boldsymbol{f}_k$ and ${}^k\boldsymbol{t}_k$, between two adjacent links are written as

$$
{}^k\boldsymbol{f}_k = \boldsymbol{R}_{k+1}^k{}^{k+1}\boldsymbol{f}_{k+1} + \boldsymbol{F}_k - m_{qk}\boldsymbol{g} + \boldsymbol{b}_k + \boldsymbol{p}_k \tag{15}
$$
$$
\begin{aligned}
{}^k\boldsymbol{t}_k = {}&\boldsymbol{R}_{k+1}^k{}^{k+1}\boldsymbol{t}_{k+1} + {}^k\boldsymbol{d}_{k/k+1} \times \boldsymbol{R}_{k+1}^k{}^{k+1}\boldsymbol{f}_{k+1} \\
&+ {}^k\boldsymbol{d}_{k/k_c} \times \boldsymbol{F}_k + \boldsymbol{T}_k + {}^k\boldsymbol{d}_{k/k_c} \times (-m_{qk}\boldsymbol{g} + \boldsymbol{p}_k) \\
&+ {}^k\boldsymbol{d}_{k/k_b} \times \boldsymbol{b}_k + \boldsymbol{n}_k
\end{aligned} \tag{16}
$$

where $\boldsymbol{R}_{k+1}^k$ is the rotation matrix that relates frame $\{k+1\}$ to frame $\{k\}$. ${}^k\boldsymbol{d}_{k/k+1}$ is the position vector from joint k to joint $k+1$, ${}^k\boldsymbol{d}_{k/k_c}$ is the position vector from the center of mass of link k to frame $\{k\}$, ${}^k\boldsymbol{d}_{k/k_b}$ is the position vector from the center of buoyancy of link k to frame $\{k\}$.

Then, the joint torques are

$$\boldsymbol{\tau}_k = \boldsymbol{z}^{T\,k}\boldsymbol{t}_k \tag{17}$$

where $\boldsymbol{z}^T$ is the unit vector along the z-axis.

In the case of ocean currents, the disturbance vector of forces and moments due to the weight and movement of the manipulator, $\boldsymbol{\sigma}_r = [\boldsymbol{\sigma}_f^T, \boldsymbol{\sigma}_m^T]^T$, can be calculated by (18-19).

$$\boldsymbol{\sigma}_f = \boldsymbol{R}_0^{B0} \boldsymbol{f}_1 \tag{18}$$

$$\boldsymbol{\sigma}_m = \boldsymbol{R}_0^{B0} \boldsymbol{t}_1 - \boldsymbol{d}_{\{B\}/\{0\}} \times (\boldsymbol{R}_0^{B0} \boldsymbol{f}_1) \tag{19}$$

where ${}^0\boldsymbol{f}_1$ and ${}^0\boldsymbol{t}_1$ are the vectors of the forces and the moments acting on the manipulator's base. $\boldsymbol{d}_{\{B\}/\{0\}}$ is the position vector from frame $\{B\}$ to frame $\{0\}$. Equations (18-19) can be rewritten in a compact form as

$$\boldsymbol{\sigma}_r = -(\boldsymbol{H}_1(\boldsymbol{q})\dot{\boldsymbol{v}}_r + \boldsymbol{C}_1(\boldsymbol{q}, \dot{\boldsymbol{q}}, \boldsymbol{v}_r)\boldsymbol{v}_r + \boldsymbol{D}_1(\boldsymbol{q}, \dot{\boldsymbol{q}}, \boldsymbol{v}_r)\boldsymbol{v}_r$$
$$+ \boldsymbol{H}_2(\boldsymbol{q})\ddot{\boldsymbol{q}} + \boldsymbol{C}_2(\boldsymbol{q}, \dot{\boldsymbol{q}})\dot{\boldsymbol{q}} + \boldsymbol{D}_2(\boldsymbol{q}, \dot{\boldsymbol{q}}, \boldsymbol{v}_r)\dot{\boldsymbol{q}} + \boldsymbol{g}_1(\boldsymbol{q})) \tag{20}$$

where $\boldsymbol{H}_1(\boldsymbol{q})$ and $\boldsymbol{H}_2(\boldsymbol{q})$ are matrices of the inertia effects due to the manipulator. $\boldsymbol{C}_i(\boldsymbol{q}, \dot{\boldsymbol{q}}, \boldsymbol{v}_r)\boldsymbol{v}_r (i = 1, 3)$ is the vector of Coriolis and centripetal forces due to the interaction between the two subsystems. $\boldsymbol{C}_2(\boldsymbol{q}, \dot{\boldsymbol{q}})\dot{\boldsymbol{q}}$ is the vector of Coriolis and centripetal forces due to the manipulator. $\boldsymbol{D}_i(\boldsymbol{q}, \dot{\boldsymbol{q}}, \boldsymbol{v}_r)$ ($i = 1 \cdots 4$) is the matrix of drag effects due to the coupling effects between the two subsystems. $\boldsymbol{g}_1(\boldsymbol{q})$ is the restoring vector due to the manipulator.

The motion equation for the manipulator part of the system under conditions of ocean currents can be written as

$$\boldsymbol{M}_m(\boldsymbol{q})\ddot{\boldsymbol{q}} + \boldsymbol{C}_m(\boldsymbol{q}, \dot{\boldsymbol{q}})\dot{\boldsymbol{q}} + \boldsymbol{D}_m(\boldsymbol{q}, \dot{\boldsymbol{q}})\dot{\boldsymbol{q}} + \boldsymbol{g}_m(\boldsymbol{q})$$
$$+ \boldsymbol{H}_2^T(\boldsymbol{q})\dot{\boldsymbol{v}}_r + \boldsymbol{C}_3(\boldsymbol{q}, \dot{\boldsymbol{q}}, \boldsymbol{v}_r)\boldsymbol{v}_r + \boldsymbol{D}_3(\boldsymbol{q}, \dot{\boldsymbol{q}}, \boldsymbol{v}_r)\boldsymbol{v}_r$$
$$+ \boldsymbol{D}_4(\boldsymbol{q}, \dot{\boldsymbol{q}}, \boldsymbol{v}_r)\dot{\boldsymbol{q}} = \boldsymbol{\tau}_m \tag{21}$$

where $\boldsymbol{H}_2^T(\boldsymbol{q})\dot{\boldsymbol{v}}_r$ is the vector of reaction forces and moments between the AUV and the manipulator. $\boldsymbol{M}_m(\boldsymbol{q})$ is the inertia matrix (including added inertia) of the manipulator. $\boldsymbol{C}_m(\boldsymbol{q}, \dot{\boldsymbol{q}})$ contains Coriolis and centripetal terms (including added Coriolis and centripetal terms) of the manipulator. $\boldsymbol{D}_m(\boldsymbol{q}, \dot{\boldsymbol{q}})$ is the hydrodynamic damping and lift matrix of the manipulator. $\boldsymbol{g}_m(\boldsymbol{q})$ is the restoring vector of the manipulator.

Then, based on (9), (20) and (21), the motion equation of the total system in the Body-fixed frame with the consideration of ocean currents can be derived as

$$\boldsymbol{M}(\boldsymbol{q}, \boldsymbol{\zeta}_r)\dot{\boldsymbol{\zeta}}_r + \boldsymbol{C}(\boldsymbol{q}, \boldsymbol{\zeta}_r)\boldsymbol{\zeta}_r + \boldsymbol{D}(\boldsymbol{q}, \boldsymbol{\zeta}_r)\boldsymbol{\zeta}_r + \boldsymbol{g}(\boldsymbol{q}, \boldsymbol{R}_I^B) = \boldsymbol{\tau} \tag{22}$$

where,

$$\boldsymbol{\zeta}_r = [\boldsymbol{v}_r^T, \dot{\boldsymbol{q}}^T]^T$$
$$\boldsymbol{M}(\boldsymbol{q}, \boldsymbol{\zeta}_r) = \begin{bmatrix} \boldsymbol{M}_v + \boldsymbol{H}_1(\boldsymbol{q}) & \boldsymbol{H}_2(\boldsymbol{q}) \\ \boldsymbol{H}_2^T(\boldsymbol{q}) & \boldsymbol{M}_m(\boldsymbol{q}) \end{bmatrix}$$
$$\boldsymbol{C}(\boldsymbol{q}, \boldsymbol{\zeta}_r) = \begin{bmatrix} \boldsymbol{C}_v(\boldsymbol{v}_r) + \boldsymbol{C}_1(\boldsymbol{q}, \dot{\boldsymbol{q}}, \boldsymbol{v}_r) & \boldsymbol{C}_2(\boldsymbol{q}, \dot{\boldsymbol{q}}) \\ \boldsymbol{C}_3(\boldsymbol{q}, \dot{\boldsymbol{q}}, \boldsymbol{v}_r) & \boldsymbol{C}_m(\boldsymbol{q}, \dot{\boldsymbol{q}}) \end{bmatrix}$$
$$\boldsymbol{D}(\boldsymbol{q}, \boldsymbol{\zeta}_r) = \begin{bmatrix} \boldsymbol{D}_v(\boldsymbol{v}_r) + \boldsymbol{D}_1(\boldsymbol{q}, \dot{\boldsymbol{q}}, \boldsymbol{v}_r) & \boldsymbol{D}_2(\boldsymbol{q}, \dot{\boldsymbol{q}}, \boldsymbol{v}_r) \\ \boldsymbol{D}_3(\boldsymbol{q}, \dot{\boldsymbol{q}}, \boldsymbol{v}_r) & \boldsymbol{D}_m(\boldsymbol{q}) + \boldsymbol{D}_4(\boldsymbol{q}, \dot{\boldsymbol{q}}, \boldsymbol{v}_r) \end{bmatrix}$$
$$\boldsymbol{g}(\boldsymbol{q}, \boldsymbol{R}_I^B) = \begin{bmatrix} \boldsymbol{g}_v(\boldsymbol{\eta}) + \boldsymbol{g}_1(\boldsymbol{q}) \\ \boldsymbol{g}_m(\boldsymbol{q}) \end{bmatrix}$$
$$\boldsymbol{\tau} = [\boldsymbol{\tau}_v^T, \boldsymbol{\tau}_m^T]^T$$
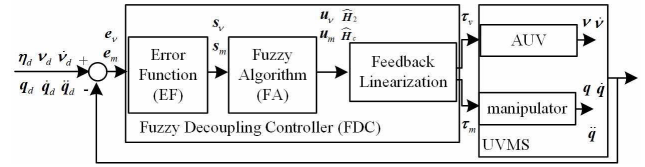

FIGURE 6. Block diagram of the fuzzy decoupling controller.

III. PROPOSED CONTROL LAW

The six-degrees-of-freedom motions of the AUV are strongly coupled. That is to say that the rotational subsystem of the AUV is coupled with translational velocities. For instance, the pitch motion has a greatly influence on the heave and surge motions, and the movement in the yaw direction affects the sway motion. Moreover, the stability of motion of the AUV at low speeds can be influenced due to the coupling effects between the manipulator and AUV. In addition, the motions of manipulator's joints are also interactive. So developing a decoupling control approach for reducing the coupling effects is of interest in this paper. The decoupling controller adopts a fuzzy algorithm to adaptively tune the gain matrix of the error function of the system. Off-diagonal elements of the gain matrix are considered. And the estimated values of the system matrices are incorporated in the controller. The whole scheme of the proposed controller is shown in Fig. 6.

A. FEEDBACK LINEARIZATION

Let's define system errors in the Body-fixed frame.

$$\boldsymbol{e} = \begin{bmatrix} \boldsymbol{e}_v \\ \boldsymbol{e}_m \end{bmatrix} = \begin{bmatrix} \boldsymbol{R}_I^B(\boldsymbol{\eta}_1 - \boldsymbol{\eta}_{1,d}) \\ \eta\boldsymbol{\varepsilon}_d - \eta\boldsymbol{\varepsilon}_d + \boldsymbol{S}(\boldsymbol{\varepsilon})\boldsymbol{\varepsilon}_d \\ \boldsymbol{q} - \boldsymbol{q}_d \end{bmatrix} \tag{23}$$

$$\dot{\boldsymbol{e}} = \begin{bmatrix} \dot{\boldsymbol{e}}_v \\ \dot{\boldsymbol{e}}_m \end{bmatrix} = \begin{bmatrix} \boldsymbol{v} - \boldsymbol{v}_d \\ \dot{\boldsymbol{q}} - \dot{\boldsymbol{q}}_d \end{bmatrix} = \boldsymbol{\zeta} - \boldsymbol{\zeta}_d \tag{24}$$

$$\ddot{\boldsymbol{e}} = \begin{bmatrix} \ddot{\boldsymbol{e}}_v \\ \ddot{\boldsymbol{e}}_m \end{bmatrix} = \begin{bmatrix} \dot{\boldsymbol{v}} - \dot{\boldsymbol{v}}_d \\ \ddot{\boldsymbol{q}} - \ddot{\boldsymbol{q}}_d \end{bmatrix} = \dot{\boldsymbol{\zeta}} - \dot{\boldsymbol{\zeta}}_d \tag{25}$$

where $\boldsymbol{\eta}_{1,d}$, $\boldsymbol{\eta}_{2,d}$, $\boldsymbol{q}_d$ and $\boldsymbol{\zeta}_d = [\boldsymbol{v}_{1,d}^T, \boldsymbol{v}_{2,d}^T, \dot{\boldsymbol{q}}_d^T]^T$ denote the desired states of $\boldsymbol{\eta}_1$, $\boldsymbol{\eta}_2$, $\boldsymbol{q}$ and $\boldsymbol{\zeta}$, respectively. $\boldsymbol{Q}_2 = \{\boldsymbol{\varepsilon}, \eta\}$ and $\boldsymbol{Q}_{2,d} = \{\boldsymbol{\varepsilon}_d, \eta_d\}$ are the quaternions of $\boldsymbol{\eta}_2$ and $\boldsymbol{\eta}_{2,d}$ respectively. Note that the attitude error of the AUV is described by the quaternion.

The error function of the system is described by the integral sliding surface function as

$$\boldsymbol{s}_v = \boldsymbol{k}_{pv}\boldsymbol{e}_v + \dot{\boldsymbol{e}}_v + \boldsymbol{k}_{iv} \int \boldsymbol{e}_v dt \tag{26}$$

$$\boldsymbol{s}_m = \boldsymbol{k}_{pm}\boldsymbol{e}_m + \dot{\boldsymbol{e}}_m + \boldsymbol{k}_{im} \int \boldsymbol{e}_m dt \tag{27}$$

where $\boldsymbol{k}_{pv}$, $\boldsymbol{k}_{iv}$, $\boldsymbol{k}_{pm}$ and $\boldsymbol{k}_{im}$ are all constant, diagonal and positive definite matrices.

To decouple the system, the dynamic equation of the UVMS in the case of ocean currents can be expressed as

$$\boldsymbol{M}_r\dot{\boldsymbol{v}}_r + \boldsymbol{H}_2\ddot{\boldsymbol{q}} + \boldsymbol{b}_v = \boldsymbol{\tau}_v \tag{28}$$

$$\boldsymbol{M}_m\ddot{\boldsymbol{q}} + \boldsymbol{H}_2^T\dot{\boldsymbol{v}}_r + \boldsymbol{b}_m = \boldsymbol{\tau}_m \tag{29}$$

where, $M_r = M_v + H_1(q)$, $[b_v^T, b_m^T]^T = C(q, \zeta_r)\zeta_r + D(q, \zeta_r)\zeta_r + g(q, R_B^I)$.

Then, the thruster forces are expressed as:

$$T = B^+ \tau_v \tag{30}$$

where

B^C

$$= \begin{bmatrix} \dfrac{r_2}{r_1 + r_2} & -\dfrac{r_5}{r_1 + r_2} & 0 & 0 & 0 & \dfrac{1}{r_1 + r_2} \\ \dfrac{r_1}{r_1 + r_2} & \dfrac{r_5}{r_1 + r_2} & 0 & 0 & 0 & -\dfrac{1}{r_1 + r_2} \\ 0 & 0 & \dfrac{r_4}{r_3 + r_4} & 0 & \dfrac{1}{r_3 + r_4} & 0 \\ 0 & 0 & \dfrac{r_3}{r_3 + r_4} & 0 & -\dfrac{1}{r_3 + r_4} & 0 \\ 0 & 1 & 0 & 0 & 0 & 0 \end{bmatrix}$$

Denote $F_{tb} = [T^T, \tau_m]^T$, where F_{tb} is the vector of thruster forces and manipulator's torques.

In terms of (28-29), the proposed control inputs are given by (31-32).

$$\tau_v = \widehat{M}_r u_v + \widehat{H}_2 \ddot{q} + \widehat{b}_v \tag{31}$$
$$\tau_m = \widehat{M}_m u_m + \widehat{H}_c \dot{v} + \widehat{b}_m \tag{32}$$

where

$$u_v = -A_v s_v - \widehat{H}_2 s_m + \dot{v}_d \tag{33}$$
$$u_m = -A_m s_m - \widehat{H}_c s_v + \ddot{q}_d \tag{34}$$

The gain matrix is expressed as

$$A = \begin{bmatrix} A_v & \widehat{H}_2 \\ \widehat{H}_c & A_m \end{bmatrix} \tag{35}$$

where $A_v, A_m, \widehat{H}_2$ and $\widehat{H}_c$ are submatrices of the gain matrix. The inclusion of off-diagonal elements in A_v constributes to decoupling of the AUV. Likewise, the decoupling of the manipulator is benifited by incorporating the off-diagonal elements in A_m. The decoupling between the AUV and the manipulator can be achieve by $\widehat{H}_2$ and $\widehat{H}_c$.

The diagonal elements of M_r and M_m are slightly influenced by the movement of the UVMS and external disturbances. And the off-diagonal elements of M_r and M_m are relatively small. Therefore, $\widehat{M}_r$ and $\widehat{M}_m$ which are the estimations of M_r and M_m are given by

$$\widehat{M}_r = \lambda_v + [\lambda_1 \theta, 0, 0, 0, \lambda_2 \theta, 0]^T \tag{36}$$
$$\widehat{M}_m = \lambda_m \tag{37}$$

where λ_v and λ_m are constant, diagonal and positive definite matrices. θ is the pitch angle. λ_1, λ_2 are constants which are both strongly depended on the relative position between the center of gravity and the center of buoyancy of the UVMS. The other off-diagonal elements in $\widehat{M}_r$ and $\widehat{M}_m$ are ignored. $\widehat{H}_2$ and $\widehat{H}_c$ could be assumed as the estimations of H_2 and H_2^T. $\widehat{b}_v$ and $\widehat{b}_m$ are estimated by $[\widehat{b}_v^T, \widehat{b}_m^T]^T = C^*(q, \zeta)\zeta + D^*(q, \zeta)\zeta + g^*(q, R_B^I)$, where $(\cdot)^*$ denotes the nominal value

that can be obtained based on strip theory, the CFD computation or the tank experiment analysis. The difference between the real value and the nominal value is denoted as the model uncertainty.

B. FUZZY ALGORITHM

Based on (31-32), it is known that the control performance largely depends on the value of the gain matrix, A. Its submatrices $A_v, A_m, \widehat{H}_2$ and $\widehat{H}_c$ are defined as shown in (38-41). In the case of strong external disturbances, the controller requires large values of the gain matrix. These high gains will result in high overshoot and even the instability of the UVMS. Besides, the UVMS is a highly coupled system. In order to avoid the problems of fixed-gain tuning and to decouple the system, the fuzzy algorithm (FA) is used to adaptively tune the gain matrix.

$$A_v = \begin{bmatrix} a_{11} & 0 & 0 & 0 & a_{15} & 0 \\ 0 & a_{22} & 0 & 0 & 0 & a_{26} \\ 0 & 0 & a_{33} & 0 & a_{35} & 0 \\ 0 & 0 & 0 & 0 & 0 & 0 \\ a_{51} & 0 & a_{53} & 0 & a_{55} & 0 \\ 0 & a_{62} & 0 & 0 & 0 & a_{66} \end{bmatrix} \tag{38}$$

$$A_m = \begin{bmatrix} a_{77} & 0 & 0 \\ 0 & a_{88} & a_{89} \\ 0 & a_{98} & a_{99} \end{bmatrix} \tag{39}$$

$$\widehat{H}_2 = \begin{bmatrix} 0 & 0 & 0 \\ a_{27} & 0 & 0 \\ 0 & a_{38} & a_{39} \\ 0 & 0 & 0 \\ 0 & a_{58} & a_{59} \\ a_{67} & 0 & 0 \end{bmatrix} \tag{40}$$

$$\widehat{H}_c = \begin{bmatrix} 0 & a_{72} & 0 & 0 & 0 & a_{76} \\ 0 & 0 & a_{83} & 0 & a_{85} & 0 \\ 0 & 0 & a_{93} & 0 & a_{95} & 0 \end{bmatrix} \tag{41}$$

where the diagonal element a_{ij} $(i = j), (i, j = 1, 2 \cdots (6 + n))$ is positive, which represents the coefficient of the *i-th* motion of the system. The off-diagonal element $a_{ij}(i \neq j)$ represents the decoupling coefficient between the *i-th* motion and the *j-th* motion. For example, a_{33} is the coefficient of the heave motion. a_{35} is the decoupling coefficient of heave motion which reduces the influence of the pitch motion on the heave motion. The meanings of other coefficients are in a similar fashion. Note that we neglect other small decoupling coefficients. And the decoupling coefficients including roll motion are neglected as well, as the roll motion is unactuated.

The input variable of the fuzzy algorithm is the absolute value of the error function $|s_i|$ $(i = 1, 2 \cdots, (6 + n))$, where $s_v = [s_1, \cdots, s_6]^T$, $s_m = [s_7, \cdots, s_{6+n}]^T$, and the output variable is a_{ij}. The general form for the *p-th* rule is:

- rule R_p: if $|s_i|$ is A_{ip} and $|s_j|$ is A_{jp} THEN a_{ii} is B_{ip}, a_{jj} is B_{jp}, a_{ij} is B_{ijp}, a_{ji} is B_{jip},

where A_{ip} and A_{jp} are the fuzzy sets for $|s_i|$ and $|s_j|$. B_{ip}, B_{jp}, B_{ijp} and B_{jip} are the fuzzy sets for a_{ii}, a_{jj}, a_{ij} and a_{ji}.
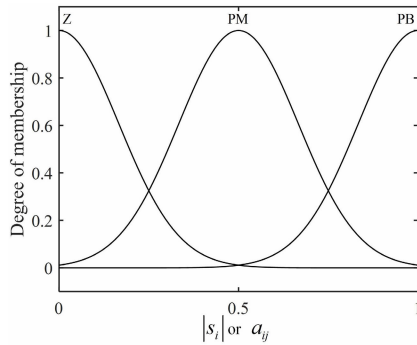
FIGURE 7. Membership function of $|s_i|$ or a_{ij}

TABLE 4. Rule base for a_{ii}.

a_{ii} \\ $|s_j|$ \\ $|s_i|$	Z	PM	PB
Z	Z	Z	PM
PM	PM	PM	PB
PB	PB	PB	PB

TABLE 5. Rule base for a_{jj}.

a_{jj} \\ $|s_j|$ \\ $|s_i|$	Z	PM	PB
Z	Z	PM	PB
PM	Z	PM	PB
PB	PM	PB	PB

TABLE 6. Rule base for a_{ij}.

a_{ij} \\ $|s_j|$ \\ $|s_i|$	Z	PM	PB
Z	Z	Z	Z
PM	Z	Z	PM
PB	Z	PM	PB

Next, we fuzzify the normalized $|s_i|$ and a_{ij} by the gaussian membership function as shown in Fig. III-B, where Z is zero, and PM is positive middle, and PB is positive big. The universe of discourse of $|s_i|$ and a_{ij} are $[0, l_{s_i}]$ and $[l_{a_{ij}}, r_{a_{ij}}]$.

Then, the Mamdani inference method and the centroid defuzzification method are used to achieve the values of normalized outputs. Finally, the actual output value a_{ij} can be obtained based on denormalization.

The parameter $a_{ij}(i = j)$ determines the slope of the error function, and the higher it is the faster will the UVMS response be. However, in practice, the gain $a_{ij}(i = j)$ can not be selected as high as desired from the view point of avoiding the oscillatory response. The parameter $a_{ij}(i \neq j)$ measures the decoupling effects, and the larger it is the greater will the disturbance be, hence an appropriate small value for $a_{ij}(i \neq j)$ is required.

Based on the above analysis, the four sets of fuzzy rules for the outputs a_{ii}, a_{jj}, a_{ij} and a_{ji} are set up as shown in Tables 4-7. The relationship between the fuzzy inputs and the fuzzy outputs are shown in Table 8.

TABLE 7. Rule base for a_{ji}.

a_{ji} \\ $|s_j|$ \\ $|s_i|$	Z	PM	PB
Z	Z	Z	Z
PM	Z	PM	PB
PB	Z	PM	PB

TABLE 8. Inputs and outputs of fuzzy variables.

inputs $|s_i|$, $|s_j|$	outputs $a_{ii}, a_{jj}, a_{ij}, a_{ji}$
$|s_1|$, $|s_5|$	$a_{11}, a_{55}, a_{15}, a_{51}$
$|s_2|$, $|s_6|$	$a_{22}, a_{66}, a_{26}, a_{62}$
$|s_3|$, $|s_5|$	$a_{33}, a_{55}, a_{35}, a_{53}$
$|s_8|$, $|s_9|$	$a_{88}, a_{99}, a_{89}, a_{98}$
$|s_2|$, $|s_7|$	$a_{22}, a_{77}, a_{27}, a_{72}$
$|s_6|$, $|s_7|$	$a_{66}, a_{77}, a_{67}, a_{76}$
$|s_3|$, $|s_8|$	$a_{33}, a_{88}, a_{38}, a_{83}$
$|s_3|$, $|s_9|$	$a_{33}, a_{99}, a_{39}, a_{93}$
$|s_5|$, $|s_8|$	$a_{55}, a_{88}, a_{58}, a_{85}$
$|s_5|$, $|s_9|$	$a_{55}, a_{99}, a_{59}, a_{95}$

C. STABILITY ANALYSIS

Comparing (28-29) and (31-32), the above mentioned control inputs lead to the following error dynamics of the UVMS.

$$-\ddot{e}_v - A_v s_v - \widehat{H}_2 s_m = \widehat{M}_r^{-1} \tau_{dv} \tag{42}$$

$$-\ddot{e}_m - A_m s_m - \widehat{H}_c s_v = \widehat{M}_m^{-1} \tau_{dm} \tag{43}$$

where τ_{dv} and τ_{dm} are the error vectors of control inputs for the AUV and the manipulator, and they combine the estimated errors such as $\widetilde{M}_r = M_r - \widehat{M}_r$, $\widetilde{b}_v = b_v - \widehat{b}_v$, $\widetilde{M}_m = M_m - \widehat{M}_m$ and $\widetilde{b}_m = b_m - \widehat{b}_m$; internal disturbances such as parameter uncertainties; and external disturbances such as ocean currents.

It can be proved that the system error $e = [e_v^T, e_m^T]^T$ is asymptotically stable on condition that the diagonal coefficients of the controller are all positive and the error vectors, τ_{dv} and τ_{dm}, are both bounded. In other words, the system travels the given desired trajectory. Besides, the chosen controller coefficients satisfy the following conditions.

$$\min\{\lambda(A_v k_{pv})\} > \left\| \frac{\partial \tau_{dv}}{e_v} \right\|, \quad \min\{\lambda(A_v)\} > \left\| \frac{\partial \tau_{dv}}{\dot{e}_v} \right\|,$$

$$\min\{\lambda(A_m k_{pm})\} > \left\| \frac{\partial \tau_{dm}}{e_m} \right\|, \quad \min\{\lambda(A_m)\} > \left\| \frac{\partial \tau_{dm}}{\dot{e}_m} \right\|.$$

where $\lambda(\cdot)$ is the function of the eigenvalue.

Therefore, $e_v \to 0$, $e_m \to 0$, and it can be observed that the tracking errors of the system are converging to zeros asymptotically.

IV. SIMULATION EXPERIMENTS
A. DESCRIPTION OF THE SIMULATING SYSTEM

Numerical simulations have been performed to explore the performance of the proposed control law on a torpedo-type

AUV (as shown in Fig.3) equipped with a three-degrees-of-freedom manipulator (as shown in Fig.4). The profile of the UVMS is shown in Fig.1. The manipulator is mounted near the bow of the AUV. The AUV has five thrusters in total, including two propulsion thrusters, two vertical thrusters and one lateral thruster, as shown in Fig.5. The manipulator is driven by brushless DC motors. The parameters of the UVMS are shown in Table 9. Hydrodynamic coefficients of the AUV are derived using strip theory. Refer to Appendix A for the details. The adjusted values of hydrodynamic coefficients are shown in Table 10.

Note that the Manipulator has negative buoyancy of $4.45N$. Even though this design brings inner disturbances to the system, it could happen in practical applications. Besides, it can be assumed that this inner disturbance is generated by the payload variations. In order to maintain the stability of a submerged body, the center of gravity (CG) should lie below the center of buoyancy (CB). For this, the AUV is designed to have the CG vertically below the CB, as shown in Fig.2. In such a way, it can be assumed that the hydrodynamic restoring forces and torques are large enough to stabilize the unactuated roll state. This means that the AUV can be exponentially stabilized through the control of only the actuated states.

To illustrate the effectiveness of the proposed controller, the comparison of the proposed FDC is made with FC and PIDID under two different tasks. To have similar comparison platform, both FC and PIDID are designed without decoupling the UVMS dynamics.

FC does not include the off-diagonal elements $a_{ij}(i \neq j)$ in gains compared to FDC, and its control input is given by

$$\boldsymbol{\tau} = \widehat{\boldsymbol{M}}(-\boldsymbol{A}\boldsymbol{s} + \dot{\boldsymbol{\zeta}}_d) + \widehat{\boldsymbol{b}} \qquad (44)$$

where $\boldsymbol{\tau} = [\boldsymbol{\tau}_v^T, \boldsymbol{\tau}_m^T]^T$, $\widehat{\boldsymbol{M}} = \text{diag}(\widehat{\boldsymbol{M}}_r, \widehat{\boldsymbol{M}}_m)$. $\boldsymbol{A}$ is the diagonal matrix such that its off-diagonal elements $a_{ij}(i \neq j)$ are zeros. $\widehat{\boldsymbol{b}} = [\widehat{\boldsymbol{b}}_v^T, \widehat{\boldsymbol{b}}_m^T]^T$.

The control inputs of PIDID are given by

$$\boldsymbol{\tau}_v = \boldsymbol{\lambda}_v(\boldsymbol{K}_{pv}\boldsymbol{e}_v + \boldsymbol{K}_{dv}\dot{\boldsymbol{e}}_v + \boldsymbol{K}_{iv}\int \boldsymbol{e}_v dt) + \boldsymbol{\tau}_{IDv} \qquad (45)$$

$$\boldsymbol{\tau}_m = \boldsymbol{\lambda}_m(\boldsymbol{K}_{pm}\boldsymbol{e}_m + \boldsymbol{K}_{dm}\dot{\boldsymbol{e}}_m + \boldsymbol{K}_{im}\int \boldsymbol{e}_m dt) + \boldsymbol{\tau}_{IDm} \qquad (46)$$

where $\boldsymbol{K}_{pv}, \boldsymbol{K}_{dv}, \boldsymbol{K}_{iv}, \boldsymbol{K}_{pm}, \boldsymbol{K}_{dm}$ and $\boldsymbol{K}_{im}$ are diagonal and positive definite matrices. $\boldsymbol{\lambda}_v$ and $\boldsymbol{\lambda}_m$ are the same with those in (36-37). $[\boldsymbol{\tau}_{IDv}^T, \boldsymbol{\tau}_{IDm}^T]^T = \boldsymbol{M}^*(\boldsymbol{q}_d, \boldsymbol{\zeta}_d)\dot{\boldsymbol{\zeta}}_d + \boldsymbol{C}^*(\boldsymbol{q}_d, \boldsymbol{\zeta}_d)\boldsymbol{\zeta}_d + \boldsymbol{D}^*(\boldsymbol{q}_d, \boldsymbol{\zeta}_d)\boldsymbol{\zeta}_d + \boldsymbol{g}^*(\boldsymbol{q}_d, \boldsymbol{R}_B^I)$, where $(\cdot)^*$ denotes the nominal value which is available for control design.

The simulations are conducted based on the following assumptions:

- Parameters of the UVMS are assumed to be inaccurate, and each parameter has about 10% inaccuracy;
- An irrotational ocean current is added in the simulation, which is assumed to be slowly varying and governed by $\boldsymbol{v}_c = [0.2\ 0.02\ 0.1\ 0\ 0\ 0]^T$ m/s;
- The fourth values of $\boldsymbol{\tau}_{IDv}$ and $\widehat{\boldsymbol{b}}_v$ are both set to be zeros as the roll motion is unactuated.

TABLE 9. Parameters of the UVMS.

Parameter	Value
AUV Mass	78.2 kg
AUV Buoyancy	771.59 N
AUV Weight	767.14 N
AUV Length	1.78 m
a_{offste}	0.003 m
a	0.15 m
b	1.17 m
c	0.49 m
c_{offste}	0.03 m
n_ν	2
β	0.523 rad
AUV Diameter	0.26 m
AUV Moments of inertia	$(0.69, 16.82, 16.82)\text{kg} \cdot \text{m}^2$
AUV Center of gravity	$(0, 0, 0)$ m
AUV Center of buoyancy	$(0, 0, 0.02)$ m
AUV Thruster Position	
r_1	0.18 m
r_2	0.18 m
r_3	0.525 m
r_4	0.245 m
r_5	0.485 m
Manipulator Mass	
m_{q1}	1.28 kg
m_{q2}	1.92 kg
m_{q3}	1.92 kg
Manipulator Buoyancy	
B_{q1}	11.43 N
B_{q2}	17.2 N
B_{q3}	17.2 N
Manipulator Weight	
W_{q1}	12.54 N
W_{q2}	18.87 N
W_{q3}	18.87 N
Manipulator Length	
l_{q1}	0.1 m
l_{q2}	0.3 m
l_{q3}	0.3 m
Manipulator Radius	
r_{q1}	0.06 m
r_{q2}	0.0425 m
r_{q3}	0.0425 m
position $\boldsymbol{p}_0^B$	$(0.6, 0, 0.2)$m
Rotation $\boldsymbol{R}_0^B$	diag$([1, 1, 1])$
Coefficient	
Linear skin drag (D_s)	0.4
Drag (C_d)	1
Lift (C_l)	0
fluid density ρ	1030

- The effects of thruster dynamics and measurement noise are not directly addressed. Thrusters are identical ones.
- The sampling time for the simulation is 2 ms.

B. TASK DESCRIPTION AND RESULTS ANALYSIS

Two different tasks have been considered for numerical simulations. And the simulation results are presented to investigate the effectiveness of the proposed fuzzy decoupling controller. The parameters of FDC, FC and PIDID are shown in Table 11. The universe of discourse of output variable considering ocean currents, a_{ij}, is given in Table 12. In addition, $l_{s_i} = 0.05\ (i = 1, 2, 3)$, $l_{s_i} = 0.087\ (i = 5, 6)$ and

TABLE 10. The values of adjusted coefficients of the AUV.

Added mass coefficients					
Force	Value	Units	Moment	Value	Units
$X_{\dot{u}}$	−2.33	Kg	$K_{\dot{p}}$	−0.3	Kg·m²/rad
$Y_{\dot{v}}$	−90.8	Kg	$M_{\dot{q}}$	−20.3	Kg·m²/rad
$Y_{\dot{r}}$	4.53	Kg·m	$M_{\dot{w}}$	−4.53	Kg·m
$Z_{\dot{w}}$	−90.8	Kg	$N_{\dot{r}}$	−20.3	Kg·m²/rad
$Z_{\dot{q}}$	−4.53	Kg·m	$N_{\dot{v}}$	4.53	Kg·m
Drag coefficients					
Force	Value	Units	Moment	Value	Units
$X_{u\|u\|}$	−2.96	Kg/m	$K_{p\|p\|}$	-0.558	Kg·m²/rad²
$Y_{v\|v\|}$	−2346	Kg/m	$M_{q\|q\|}$	−807	Kg·m²/rad²
$Y_{r\|r\|}$	0.759	Kg·m/rad²	$M_{w\|w\|}$	8.76	Kg
$Z_{w\|w\|}$	−242	Kg/m	$N_{r\|r\|}$	−404	Kg·m²/rad²
$Z_{q\|q\|}$	−0.759	Kg·m/rad²	$N_{v\|v\|}$	−8.76	Kg
Lift coefficients					
Force	Value	Units	Moment	Value	Units
Y_{uv}	−56.5	Kg/m	M_{uq}	−8.9	Kg·m/rad
Y_{ur}	11.8	Kg/rad	M_{uw}	−24.9	Kg
Z_{uw}	−56.5	Kg/m	N_{ur}	−8.9	Kg·m/rad
Z_{uq}	−11.8	Kg/rad	N_{uv}	24.9	Kg

FIGURE 8. Comparative 3-D trajectory tracking results of the AUV duirng task 1.

TABLE 11. Controller parameter setting for simulations.

Auv controller	Value
$k_{p\nu}$	diag(1.2, 1.2, 1.2, 0, 5, 5)
$k_{i\nu}$	diag(1, 1, 1, 0, 1, 1)
λ_1	4.84
λ_2	15
λ_ν	diag(86, 179, 174, 0, 46, 46)
$K_{p\nu}$	diag(6, 6, 10, 0, 15, 15)
$K_{i\nu}$	diag(4, 4, 4, 0, 6, 6)
$K_{d\nu}$	diag(4, 4, 8, 0, 12, 12)
Manipulator controller	Value
k_{pm}	diag(5, 20, 12)
k_{im}	diag(2, 5, 3)
λ_m	diag(1.4, 0.88, 0.11)
K_{pm}	diag(30, 40, 135)
K_{im}	diag(10, 20, 30)
K_{dm}	diag(5, 5, 5)

$l_{s_i} = 0.52$ $(i = 7, 8, 9)$. It is noted that the same values of the controller parameters are used throughout the two tasks, except some off-diagonal values in Table 12.

1) TASK 1 AND RESULTS ANALYSIS

The first task is that the AUV is asked to track a given spatial trajectory, and the manipulator maintains in its initial configuration. In this condition, the AUV accelerates for the initial 20 s and attains surge velocity of 1 m/s ($\approx$ 2 knots). Then, it maintains uniform motion within the following 100 s and decelerates to zero velocity for the final 20 s. In addition, other main motions, such as heave down and up and sway in and out, are included in the desired spatial trajectory of the AUV as well. This task is performed to identify the interaction between the AUV and the manipulator during the AUV motion in the presence of parameter uncertainties and external disturbances.

Here, two cases have been considered to design the desired trajectory of the AUV. Moreover, the effects of ocean currents are considered as well. In case 1 (c1), the coupling effects between the sway and yaw motions and the coupling effects between the heave and pitch motions are both considered. The desired trajectories of the yaw motion and the pitch motion are designed in accordance with the sway motion and the heave motion, respectively. During the sway in motion from zero to 7.5 m and the sway out motion from 7.5 m to zero, the yaw angle accelerates for the initial 20 s and attains 9°, and then the yaw motion undergoes deceleration stage and acceleration stage for 40 s-80 s and attains −9°, and it decelerates to zero for the final 20 s, as shown in Fig.10 (*a*) and (*c*). In such a way, the movement of yaw motion is coordinated with the motions from sway in to sway out in the presence of ocean currents. During the heave down motion from zero to 7.5 m and the heave up motion from 7.5 m to zero, the pitch angle accelerates for the initial 20 s and attains −1.15°, and then the pitch angle undergoes deceleration stage and acceleration stage for 40 s-80 s and attains 11.5°, and it decelerates to zero for the final 20 s, as shown in Fig.10 (*e*) and (*g*). In such a way, the movement of pitch motion is coordinated with the motions from heave down to heave up in the presence of ocean currents. The average values of sway and heave velocities are both 0.125m/s ($\approx$ 0.25 knots). The average values of angular velocities of yaw and pitch motions are 0.008 rad/s and 0.01 rad/s.

In case 2 (c2), only the coupling effects between the sway and yaw motions are considered. The yaw angle is the same with that in case 1, while the pitch angle is chosen to be zero.

In the two cases, the manipulator's links are arranged to be folded. In such a way, the influences of the manipulator on the AUV are small. And manipulator's joint angles are $q_1 = 180°$, $q_2 = 0°$ and $q_3 = 180°$. The FDC is performed on the two cases termed as: FDC_{c1} and FDC_{c2}. And the FC and PIDID are performed only on case 1, which are termed as FC_{c1} and $PIDID_{c1}$.

Fig.8 shows the desired 3-D trajectory and tracking control results of the AUV based on FDC_{c1}, FC_{c1} $PIDID_{c1}$ and FDC_{c2}. The tracking control results of motions of the AUV and the corresponding tracking errors given by the controllers can be observed in Fig.9-Fig.11. The simulation results based on FDC_{c1} are presented in Fig.12. These results illustrate

TABLE 12. Universe of discourse for output variable a_{ij} (where $\cdot/\cdot$ denotes that the values before / are for task 1 and the values behind / are for task 2)).

$(l_{a_{ij}}, r_{a_{ij}})\backslash j$ i	1	2	3	4	5	6	7	8	9
1	(5, 15)	*	*	*	(0, −15)	*	*	*	*
2	*	(5, 15)	*	*	*	(−20, −10)/(0, −10)	(0, 0.1)	*	*
3	*	*	(8, 15)	*	(5, 0)/(0, 1)	*	*	(0, 1)	(0, 0.1)
4	(0, 5)	*	*	*	*	*	*	(0, 0.1)	(0, 0.1)
5	*	(0, 30)/(40, 30)	(10, −20)/(−15, −20)	*	(5, 15)	*	*	*	*
6	*	(−1, 0)	*	*	*	(5, 15)	(0, 0.1)	*	*
7	*	*	*	*	*	(−1, 0)	(1, 16)	*	*
8	*	*	(0, 2)	*	(0, 2)	*	*	(0, 3)	(0, 1)/(0, 2)
9	*	*	(2, 0)	*	(2, 0)	*	*	(5, 3)/(6, 2)	(8, 16)

TABLE 13. Performance measure (IAE, ITAE) on task 1.

Control scheme	x	y	z	ϕ	θ	ψ	q_1	q_2	q_3
PIDID_{c1}	(1.66, 67.8)	(1.66, 83.9)	(0.99, 53.4)	(15.9, 1082)	(1.99, 98.4)	(1.23, 62.9)	(0.68, 38.5)	(1.05, 47.1)	(4.89, 253)
FC_{c1}	(0.74, 27.8)	(0.76, 39.4)	(0.38, 19.6)	(15.8, 1081)	(1.18, 61.5)	(0.84, 43.4)	(0.42, 22.1)	(0.20, 9.34)	(2.54, 134)
FDC_{c1}	(0.72, 24.5)	(0.55, 30.9)	(0.36, 19.2)	(15.8, 1080)	(0.83, 45.6)	(0.35, 17.7)	(0.36, 19.8)	(0.17, 8.6)	(2.52, 130)
FDC_{c2}	(0.73, 25.6)	(0.67, 41.2)	(0.46, 27.7)	(16.2, 1116)	(0.86, 50.0)	(0.32, 15.7)	(0.32, 15.9)	(0.20, 10.9)	(2.42, 109)

Note: $\text{IAE} = \int_0^t ||e_\xi||dt$ and $\text{ITAE} = \int_0^t t \cdot ||e_\xi||dt$, where e_ξ is the system errors and $e_\xi = [\boldsymbol{\eta}_d^T, \boldsymbol{q}_d^T]^T - [\boldsymbol{\eta}^T, \boldsymbol{q}^T]^T$
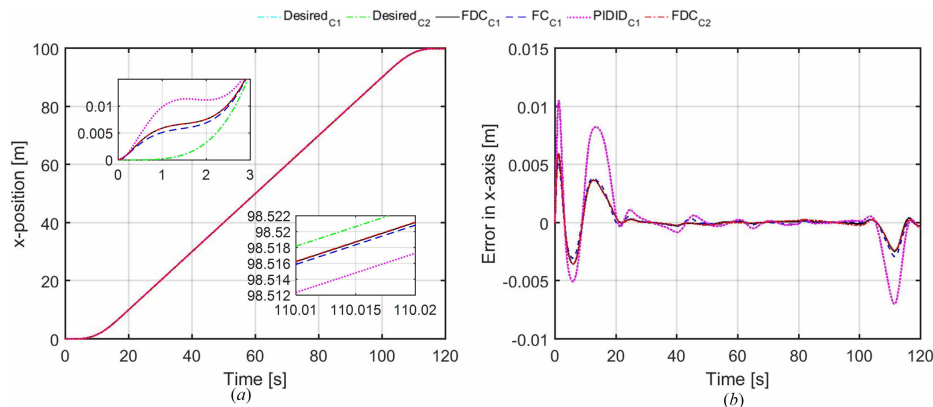
FIGURE 9. Comparisons of trajectory tracking results and tracking errors during task 1 (*a*) tracking results in *x*-axis, (*b*) tracking errors in *x*-axis.

that the three controllers in two cases are all good to track a given spatial trajectory. From these figures, it is observed that, the tracking errors of surge, sway and heave motions are within ± 0.015 m, ± 0.005 m and ± 0.005 m; and the tracking errors of yaw and pitch motions are within $\pm 0.5°$; and the errors of roll, q_1, q_2 and q_3 are within $\pm 2.5°$, $\pm 0.5°$, $\pm 1.5°$ and $\pm 1.5°$; which are all within the design limits (± 0.02 m and $\pm 8°$ in positions and orientations, respectively). During the vehicle trajectory tracking, the surge, yaw, pitch and roll motions of the vehicle are greatly influenced by the dynamic coupling between degrees of freedom of the vehicle, by the manipulator inclusion, and also by the external disturbances such as ocean currents. The proposed control scheme FDC_{c1} and FDC_{c2} outperform FC_{c1} which compensates these coupling and disturbance effects simply by adopting off-diagonal elements $a_{ij}(i \neq j)$ in the gain matrix. And the results of PIDID_{c1} are inferior to those obtained when using FC_{c1}, as we adopt the fuzzy algorithm

to adaptively tune the diagonal coefficients $a_{ij}(i = j)$ in the gain matrix. As observed from Fig.10 (*f*) and (*h*), an initial pitch angle variation drifts occur in the heave direction during task 1 (during acceleration stage). Besides, the vehicle motion and external disturbances cause the initial joints 1, 2 and 3 angles variation drifts during the acceleration stage of task 1 (refer to Fig. 11 (*b*)-(*d*)). However, these unwanted effects are successfully compensated in the proposed control scheme and therefore tracking errors are within their design limits. In addition, in order to sustain the effectiveness of the proposed controller, a quantitative analysis is done based on integral of the absolute error (IAE) and integral of the time absolute error (ITAE), as shown in Table 13. Form these indices, it is to be noted that FDC_{c1} provides reduced tracking errors in comparison with FC_{c1}, PIDID_{c1} and FDC_{c2} schemes.

The thruster forces and manipulator's torques on individual components of the UVMS are presented in Fig.13.
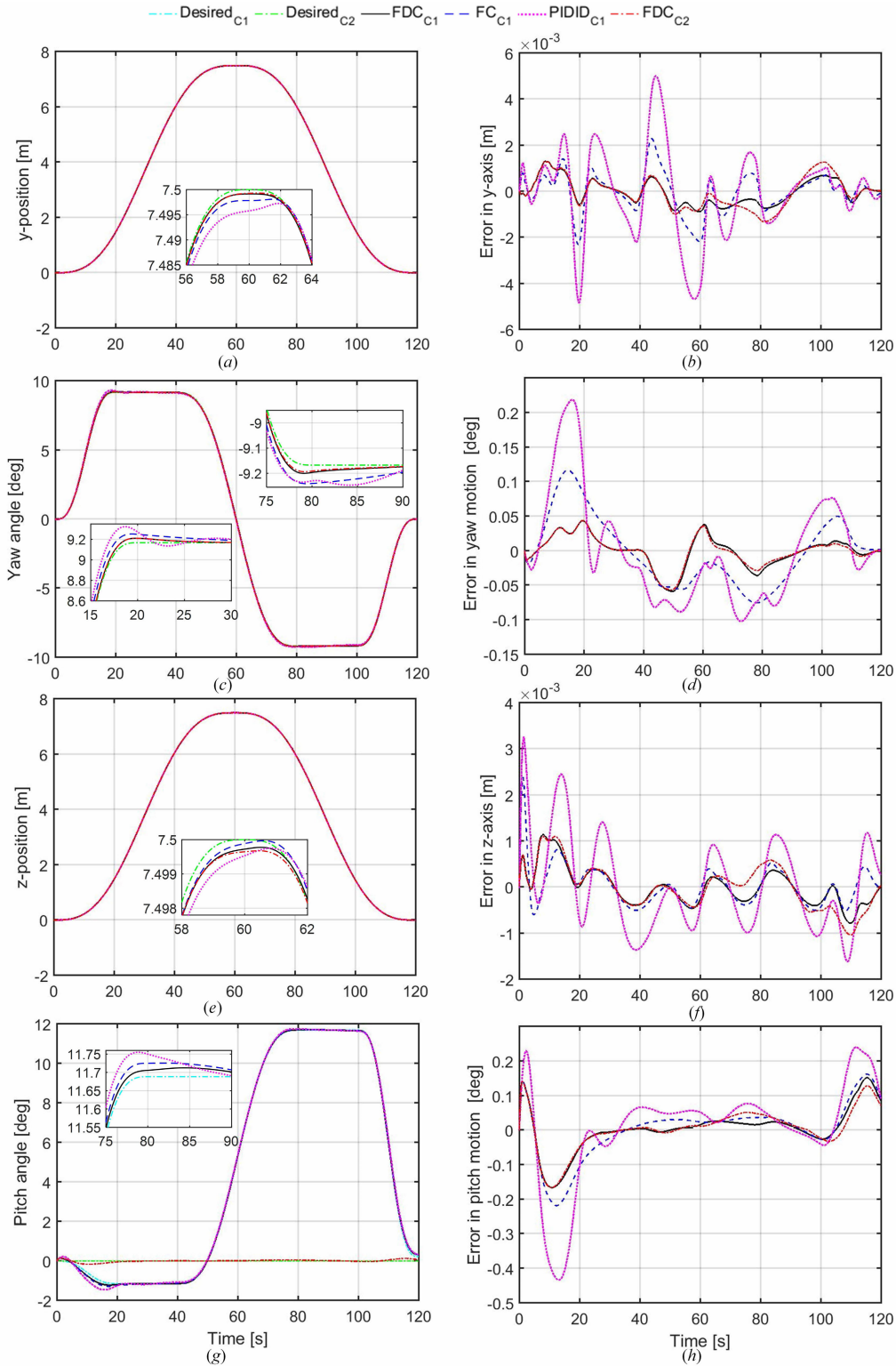
FIGURE 10. Comparisons of trajectory tracking results and tracking errors of *y*, yaw, *z* and pitch motions during task 1 ((*a*) tracking results in *y*-axis, (*b*) tracking errors in *y*-axis, (*c*) tracking results in yaw motion, (*d*) tracking errors in yaw motion, (*e*) tracking results in *z*-axis, (*f*) tracking errors in *z*-axis, (*g*) tracking results in pitch motion, (*h*) tracking errors in pitch motion).

Fig.14 reports the time history of the 2-norm of the vector of total thruster forces and manipulator's torques ($\boldsymbol{F}_{tb} =$ $[\boldsymbol{T}^T, \boldsymbol{\tau}_m^T]^T$). For the sake of argument, Table 14 reports the time integral of the 2 norms of vector $\boldsymbol{F}_{tb}$ obtained in Task 1
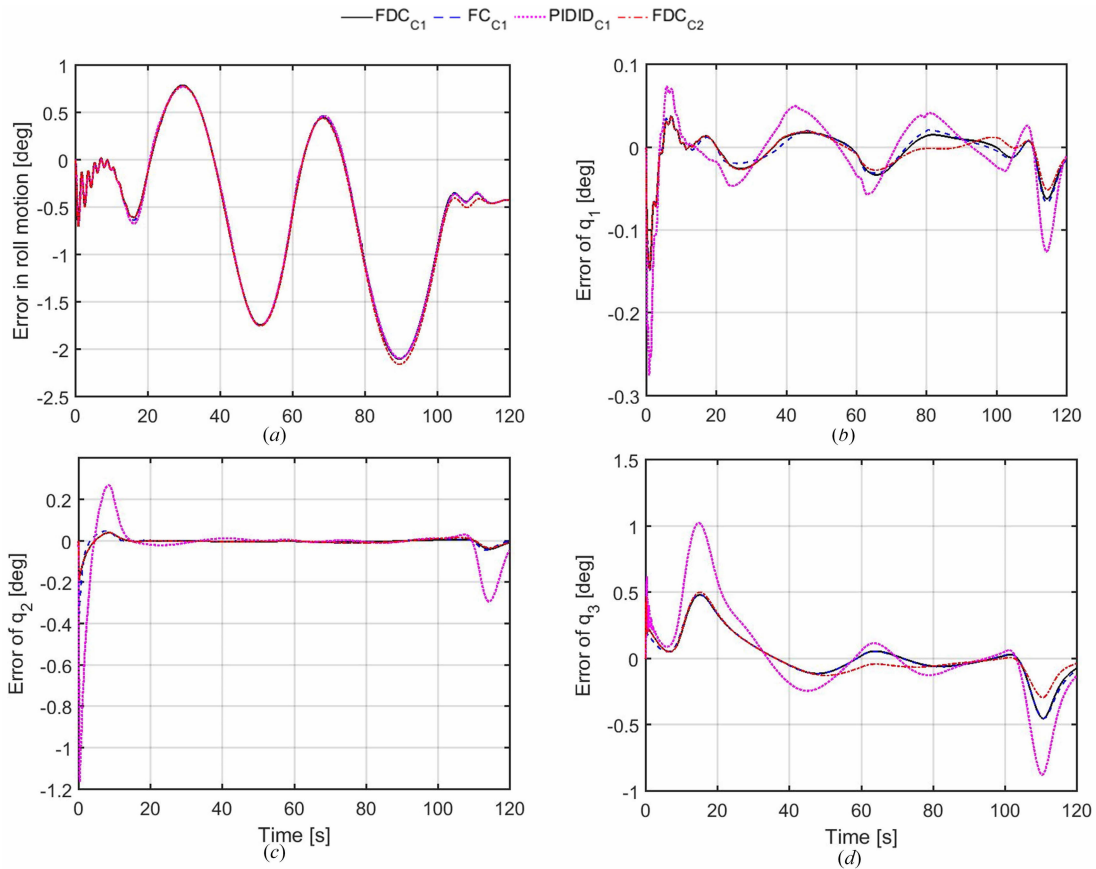
FIGURE 11. Comparative errors of AUV roll motion and manipulator's joints during task 1 ((a) Errors in roll motion, (b) errors of q_1, (c) errors of q_2, (d) errors of q_3).
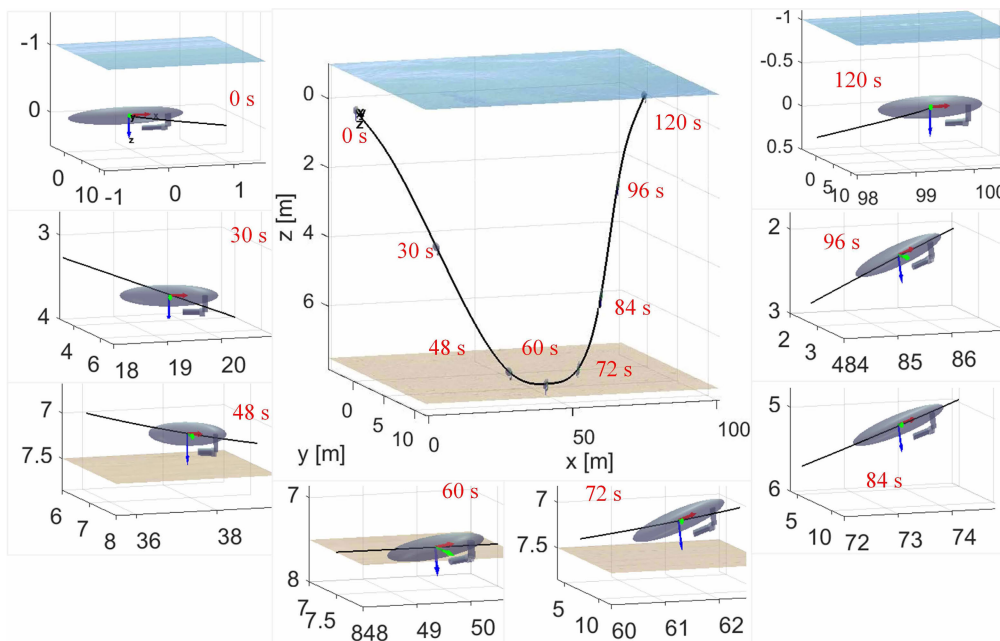
FIGURE 12. Simulation results of the proposed method (FDC_{C1}) during task 1.

simulations over a 120 s duration. It is easy to recognize that during Task 1, case 1 (c1) are less energy-consuming than

case 2 (c2). Moreover, the reduced energy consumption may be expected to result in decreasing in energy consumption
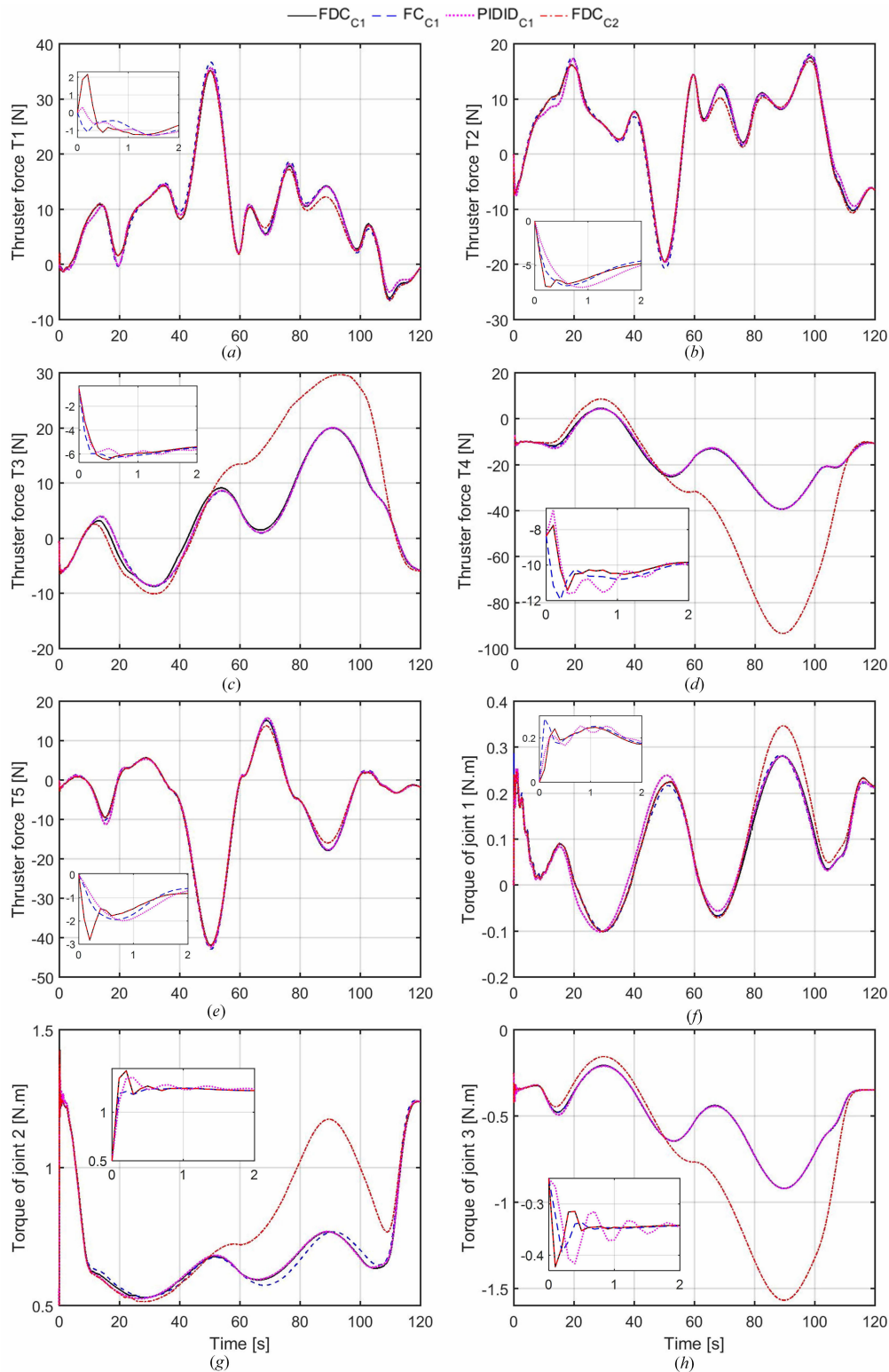
FIGURE 13. Thruster forces and manipulator's torques during task 1 ((*a*) thruster force of T_1, (*b*) thruster force of T_2, (*c*) thruster force of T_3, (*d*) thruster force of T_4, (*e*) thruster force of T_5, (*f*) torque of joint T_{q1}, (*g*) torque of joint T_{q2}, (*h*) torque of joint T_{q3}).

for an autonomous UVMS, which is a remarkable advantage because of energy storage limitations of AUVs. Therefore,

the proposed decoupling trajectory ((c1)) becomes the more attractive the longer is the duration of the manipulative task.

TABLE 14. Time integral of the 2-norm of the thruster forces and manipulator's torques in task 1.

Control scheme	PIDID_{c1}	FC_{c1}	FDC_{c1}	FDC_{c2}
$\int \lVert \boldsymbol{F}_{tb} \rVert dt$	3373.279	3395.927	3391.392	5399.166
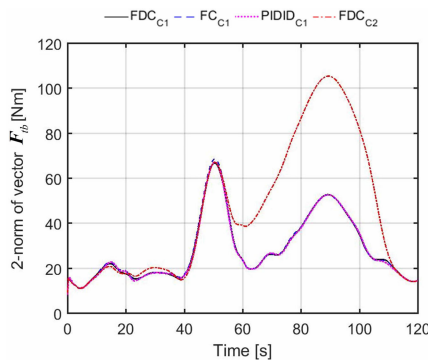
FIGURE 14. Time history of the 2-norm of the thruster forces and manipulator's torques vector (F_{tb}) in task 1.

FIGURE 15. Comparative tracking results of manipulator's end-effector during task 2.

FIGURE 16. Simulation results of the proposed method (FDC) during task 2.

In addition, it is observed that the thruster forces in FDC_{c1} are approximately within $\pm 50N$ and the joint torques are within $\pm 2Nm$, which are well within the limits for the chosen thrusters and actuators. It is worth noting that external disturbances such as larger time-varying ocean currents are difficult to be adapted in the PIDID scheme based on the simulation results (which are not included in this paper due to the limited space).

All in all, it is evident that with respect to the above two measures, FDC_{c1} outperforms FC_{c1}, PIDID_{c1} and FDC_{c2} in terms of robustness to parameter uncertainties and ocean currents, and provides superior performance in terms of tracking errors and energy consumption.

2) TASK 2 AND RESULTS ANALYSIS

In the second task, the AUV maintains station keeping and the manipulator has a repeated desired trajectory. This task is performed to identify the station keeping ability of the AUV during the movement of manipulator in the case of parameter uncertainties and external disturbances. The initial velocities and positions of the AUV are chosen to be zeros. And the initial joint angles of the manipulator are arranged to be $q_1 = 0°$, $q_2 = 40°$ and $q_3 = 45°$. The initial joint velocities are zeros. And the desired joint angles are as follows. q_{1d}

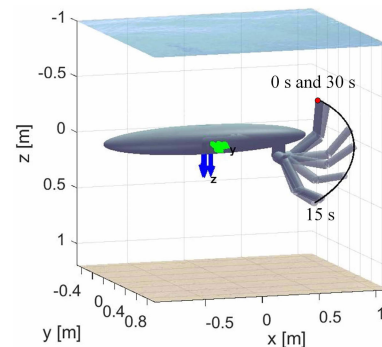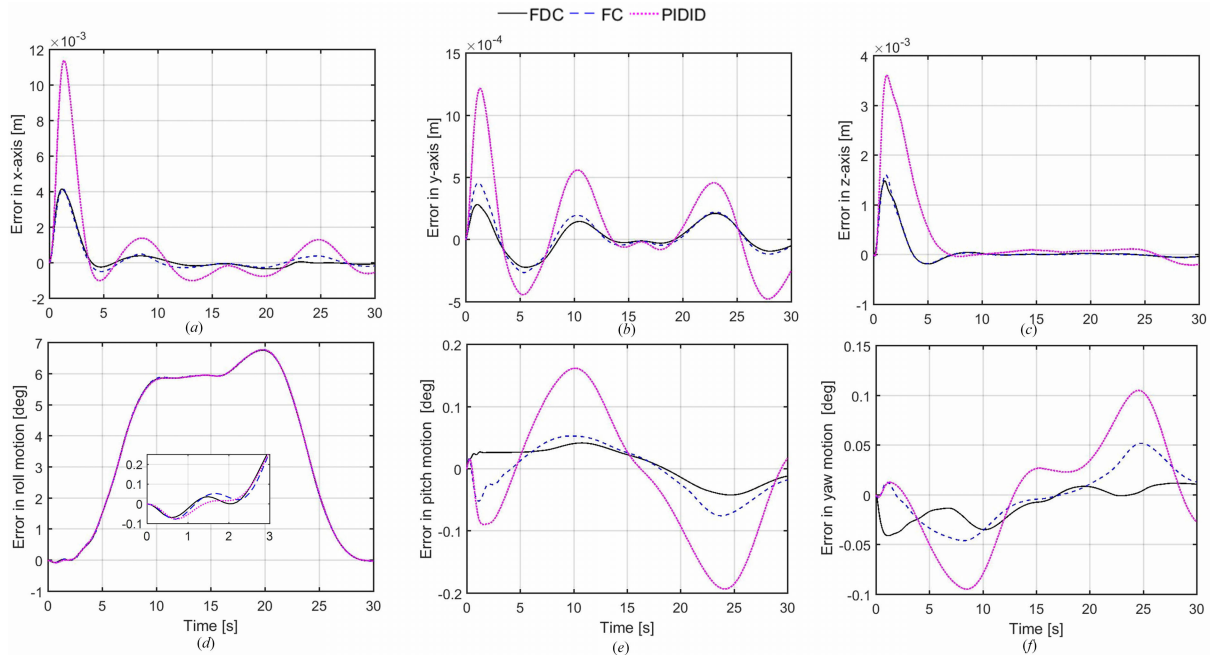accelerates from $0°$ to $86°$ in the initial 15 s and decelerates to zero in the following 15 s. q_2 rotates from $40°$ to $-46°$ in the initial 15 s and then rotates to $40°$ in the following 15 s. And $q_{3d} = 45°$. The average angular velocities of q_1 and q_2 are both 0.06 rad/s.

The desired manipulator's end-effector trajectory and control tracking results based on three methods are given in Fig.15. Fig.16 reports the simulation results based on the proposed method (FDC). These results illustrate that the three controllers are all good enough to track the desired repeated trajectory. From Fig.17-Fig.18, it is observed that based on the three controllers the errors of surge, sway and heave motions are within ± 0.015 m, ± 0.005 m and ± 0.005 m; and the errors of roll, pitch and yaw motions are within $8°$, $\pm 0.2°$ and $\pm 0.2°$; and the tracking errors of q_1, q_2 and q_3 are within $\pm 1.5°$, $\pm 3°$ and $\pm 3°$; which are all within the design limits (± 0.02 m and $\pm 8°$ in positions and orientations, respectively). From Fig.17, it can be observed

TABLE 15. Performance measure (IAE, ITAE) on task 2.

Control scheme	x	y	z	ϕ	θ	ψ	q_1	q_2	q_3
PIDID	(0.39, 3.20)	(0.09, 1.18)	(0.12, 0.64)	(19.3, 300)	(0.48, 7.73)	(0.24, 3.90)	(2.43, 38.9)	(2.13, 24.2)	(2.25, 28.4)
FC	(0.13, 0.89)	(0.04, 0.44)	(0.03, 0.14)	(19.3, 300)	(0.22, 3.65)	(0.17, 2.78)	(1.75, 27.5)	(1.52, 17.5)	(1.49, 18.3)
FDC	(0.12, 0.67)	(0.02, 0.35)	(0.03, 0.14)	(19.3, 299)	(0.14, 2.00)	(0.03, 0.30)	(1.75, 27.4)	(1.28, 14.1)	(0.81, 10.1)

Note: IAE=$\int_0^t \lVert e_\xi \rVert dt$ and ITAE=$\int_0^t t \cdot \lVert e_\xi \rVert dt$, where e_ξ is the system errors and $e_\xi = [\boldsymbol{\eta}_d^T, \boldsymbol{q}_d^T]^T - [\boldsymbol{\eta}^T, \boldsymbol{q}^T]^T$

FIGURE 17. Comparative errors of AUV motion during task 2 ((*a*) errors in *x*-axis, (*b*) errors in *y*-axis, (*c*) errors in *z*-axis, (*d*) errors in roll motion, (*e*) errors in pitch motion, (*f*) errors in yaw motion).
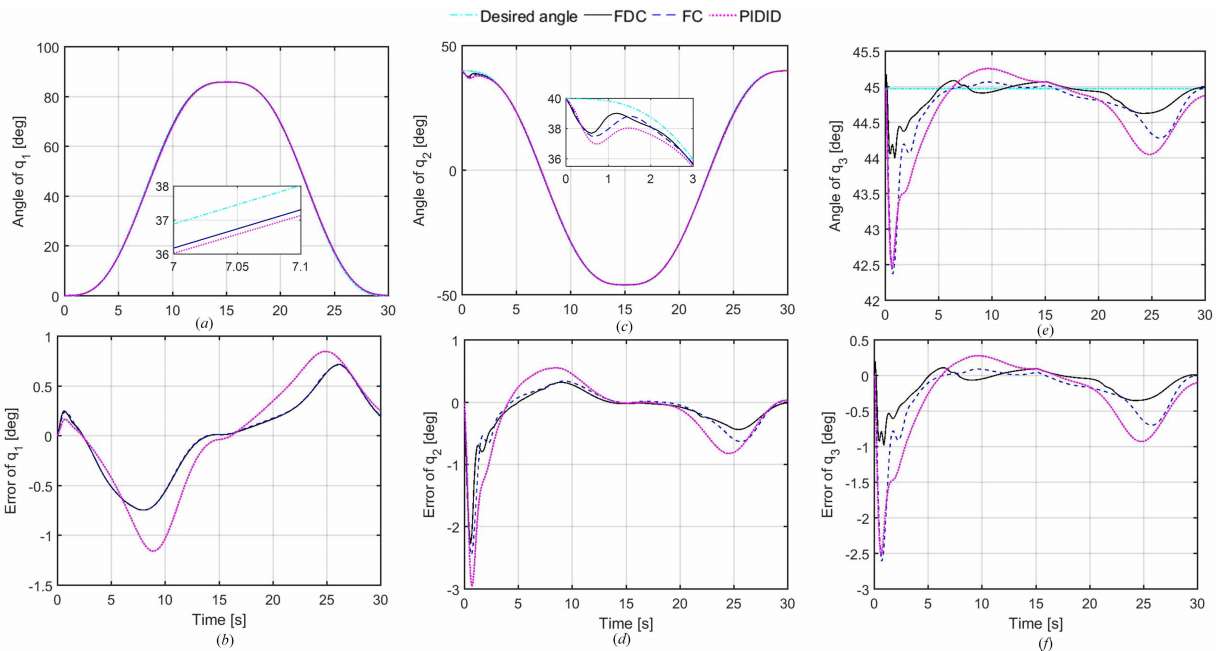
FIGURE 18. Comparisons of tracking results and tracking errors of the manipulator in task 2 ((*a*) tracking results in q_1, (*b*) tracking errors in q_1, (*c*) tracking results in q_2, (*d*) tracking errors in q_2, (*e*) tracking results in q_3, (*f*) tracking errors in q_3).

that the vehicle state errors are minimized in the proposed control scheme (FDC) by adopting a fuzzy algorithm to adaptively tune the gain matrix with off-diagonal elements for the reduction of the interaction effects. As observed from Fig.18 (*d*) and (*e*), the coupling effects and external disturbances cause an initial joints 2 and 3 angle variation drifts during the manipulator motion. However these unwanted effects are better compensated in the proposed control scheme (FDC)

than in the FC and PIDID. From the overall results, it is observed that the UVMS is affected by parameter uncertainties, external disturbances; however, FDC provides better station-keeping performance of the AUV and better trajectory tracking performance of the manipulator compared to FC, and the performance of FC is better than that of PIDID. This can be verified by quantifiable analysis as shown in Table 15. From Fig.19, it is known that the thruster forces are within
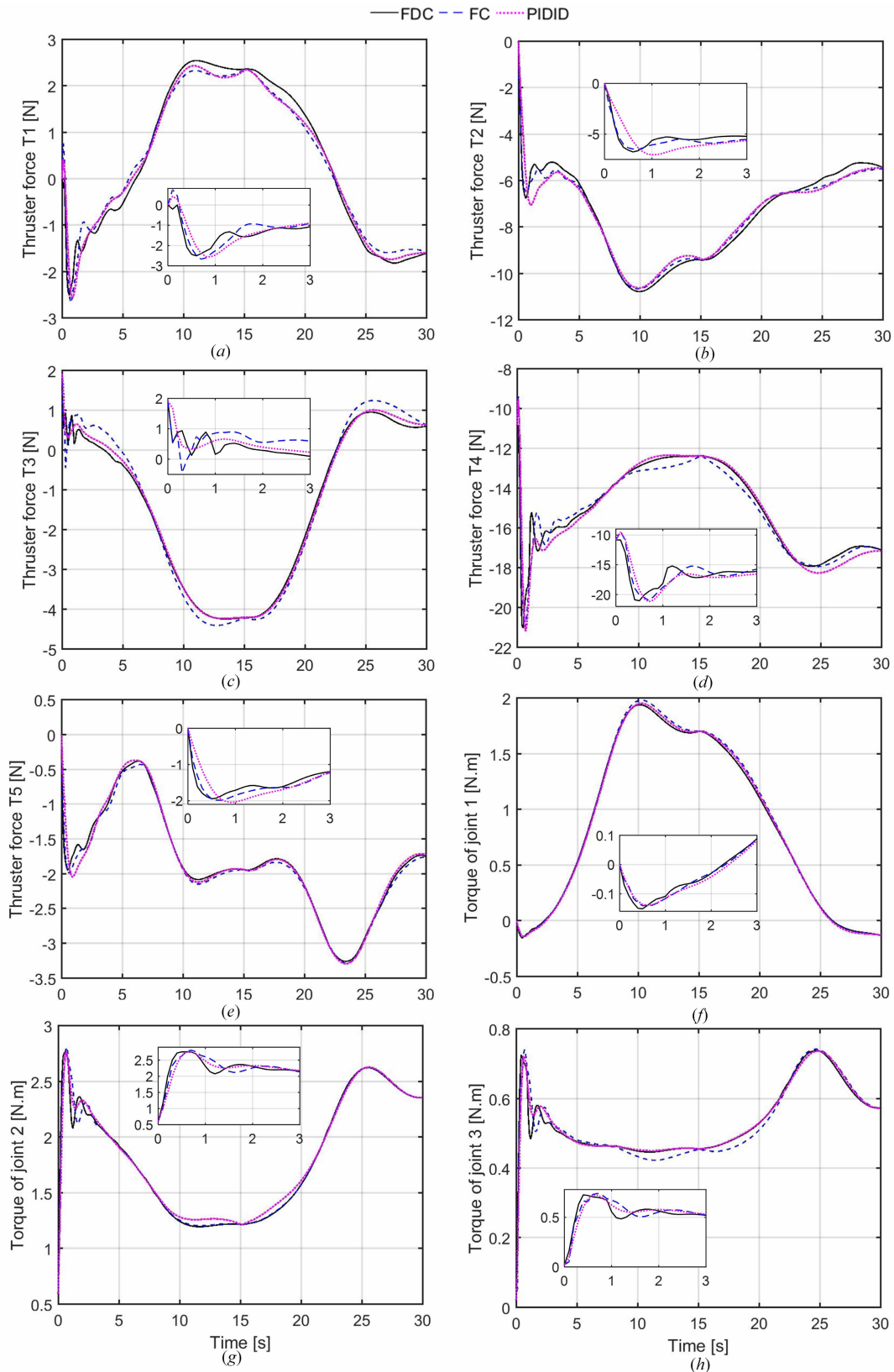
FIGURE 19. Thruster forces and manipulator's torques during task 2 ((*a*) thruster force of T_1, (*b*) thruster force of T_2, (*c*) thruster force of T_3, (*d*) thruster force of T_4, (*e*) thruster force of T_5, (*f*) torque of joint T_{q1}, (*g*) torque of joint T_{q2}, (*h*) torque of joint T_{q3}).

±25 N, and the joint torques are within ±3 N·m, which are well within the ranges of the chosen thrusters and actuators.

In terms of the above simulation results under the two tasks, it is concluded that compared to PIDID, FC takes advantages of the fuzzy algorithm to adaptively tune the gain matrix. Moreover, compared to FC, FDC takes advantages of the inclusion of the off-diagonal elements in the gain matrix to further decouple the system on the condition of parameter uncertainties and external disturbances. In addition, the thruster forces and manipulator's torques can be reduced through designing a decoupling trajectory (case 1) for the AUV in consideration of both the coupling effects between the sway and yaw motions and the coupling effects between the heave and pitch motions.

In this paper, the motor dynamics of the manipulator actuators are not considered, as we assumed that the manipulator is driven by brushless DC motors. Consequently, it is supposed that the motor's torques of manipulator actuators are applied without any delay. During this study, the effects of measurement noise are not addressed. It is assumed that the noise and drift generated by the inertial sensors do not have considerable effect on control performance [18]. That's because of the fact that the rate gyroscopes and accelerometers are low-noise and fast-dynamics sensors and the further assumptions that some auxiliary equipment, e.g. magnetometers [42] are used to compensate for the gyroscope drift and a suitable terrain aided underwater navigation technique [43] is applied to compensate for the accelerometer drift. In the simulations, the sampling time for simulation is 2 ms (i.e. sampling frequency is 500 HZ). In this case, the control algorithm is insensitive to the time-step value provided that the sampling frequency is chosen to be not less than ten times the maximum frequency parameter of the controller.

V. CONCLUSION

In this work, the most dominating hydrodynamic coefficients for a torpedo-type AUV are derived using strip theory and are adjusted according to dynamical similarity, which provides a new solution for obtaining the more accurate hydrodynamic coefficients. The dynamic model of the UVMS with closed-form equations provides an insight into the coupling effects between the two subsystems and the coupling effects between degrees-of-freedom of the subsystem. Having a clear understanding of the interaction is beneficial for designing the proposed fuzzy decoupling controller. The gain matrix including off-diagonal elements tuned by a fuzzy algorithm is incorporated into the control strategy to decouple the system. This scheme possesses robustness to parameter uncertainties and external disturbances. The desired trajectory of the AUV in consideration of the coupling effects between degrees of freedom of the AUV is designed. Comparing with the simulation results of the traditional fuzzy controller (FC) and the conventional PID controller with the inverse dynamic model (PIDID), it is demonstrated the superior performance of the proposed method (FDC) in terms of tracking error norm. Comparing with the simulation results in the case 2, it is

demonstrated the superior performance in the case 1 in terms of energy consumption. This technique can be extended to the other vehicle states since the insight into the coupling effects is provided.

This paper has been verified by numerical simulations alone. Even though this is an important first step, actual underwater experiments must be conducted to understand the challenges associated with the implementation of our proposed fuzzy decoupling controller. And it is crucial that the suitability and the advantages of our proposed control scheme are experimental validated. Nevertheless, the development of an experimental system for an UVMS is commonly expensive, which is an obstacle to performing the experimental analysis. For field experiments at sea, in addition to the development of an experimental UVMS, it is necessary to adopt a support ship to carry the experimental UVMS to an experimental site. And researchers on the support ship could observe and communicate with the experimental UVMS. Even with the pool experiments, a large water tank is required. Therefore, it would be useful to perform computer simulations to justify the effectiveness of the proposed control approach before the experiments in the pool or at sea, which not only saves on the cost and time needed but also reduces the risks encountered when the control system is finally implemented in hardware. The extensive underwater experiments on the proposed controller would be conducted when an autonomous UVMS becomes available in the future.

APPENDIXES
APPENDIX A
COEFFICIENT DERIVATION
A. ADDED MASS COEFFICIENTS
1) AXIAL ADDED MASS
To estimate the axial added mass, the vehicle hull shape is approximated by an ellipsoid shown in Fig.2. The following empirical formula of the axial added mass is given in [44].

$$X_{\dot{u}} = -\frac{4\alpha\rho\pi}{3}(\frac{l}{2})(\frac{d}{2})^2 \qquad (47)$$

where ρ is the density of the surrounding fluid. α is empirical parameter determined by the ratio of vehicle length l to diameter d. When $\frac{l}{d} = 7$, α is measured as 0.03585 by Blevins [44]. The final value of $X_{\dot{u}}$ is given in Table 18.

2) CROSSFLOW ADDED MASS
Strip theory is used to calculate the added mass of vehicle. The added mass of per unit length of a single cylindrical slice is given in [10] as

$$m_a(x) = \pi\rho R(x)^2 \qquad (48)$$

where $R(x)$ is the hull radius given by (1-2), which is a function of axial position.

The added mass of a circle with fins is given in [44] as:

$$m_{af}(x) = \pi\rho a_{\text{fin}}^2(1 - \frac{R(x)^2}{a_{\text{fin}}^2} + \frac{R(x)^4}{a_{\text{fin}}^4}) \qquad (49)$$

TABLE 16. AUV fin parameters.

Parameter	value	Description
S_{fin}	9.68×10^{-3} m^2	Planform Area
x_{fin}	-0.758 m	fin $x-$position wrt $\{B\}$
a_{fin}	0.198 m	Max fin height above centerline
c_{df}	0.585	Fin drag coefficient
c_{lf}	3.11	Fin lift coefficient

TABLE 17. AUV hull coordinates for limits of integration.

Parameter	value	Description
x_t	-0.945 m	Aft end of tail section
x_{t2}	-0.485 m	Forward end of tail section
x_f	-0.823 m	Aft end of fin section
x_{f2}	-0.753 m	forward end of fin section
x_b	0.658 m	aft end of bow section
x_{b2}	0.835 m	forward end of bow section
x_{cg}	-0.835 m	CG wrt origin at vehicle nose

TABLE 18. The values of coefficients calculated based on strip theroy.

Added mass coefficients					
Force	Value	Units	Moment	Value	Units
$X_{\dot{u}}$	-2.33	Kg	$K_{\dot{p}}$	-0.07	Kg·m^2/rad
$Y_{\dot{v}}$	-90.8	Kg	$M_{\dot{q}}$	-20.3	Kg·m^2/rad
$Y_{\dot{r}}$	4.53	Kg·m	$M_{\dot{w}}$	-4.53	Kg·m
$Z_{\dot{w}}$	-90.8	Kg	$N_{\dot{r}}$	-20.3	Kg·m^2/rad
$Z_{\dot{q}}$	-4.53	Kg·m	$N_{\dot{v}}$	4.53	Kg·m
Drag coefficients					
Force	Value	Units	Moment	Value	Units
$X_{u\|u\|}$	-2.96	Kg/m	$K_{p\|p\|}$	-0.0154	Kg·m^2/rad^2
$Y_{v\|v\|}$	-242	Kg/m	$M_{q\|q\|}$	-35	Kg·m^2/rad^2
$Y_{r\|r\|}$	0.759	Kg·m/rad^2	$M_{w\|w\|}$	8.76	Kg
$Z_{w\|w\|}$	-242	Kg/m	$N_{r\|r\|}$	-35	Kg·m^2/rad^2
$Z_{q\|q\|}$	-0.759	Kg·m/rad^2	$N_{v\|v\|}$	-8.76	Kg
Lift coefficients					
Force	Value	Units	Moment	Value	Units
Y_{uv}	-56.5	Kg/m	M_{uq}	-8.9	Kg·m/rad
Y_{ur}	11.8	Kg/rad	M_{uw}	-24.9	Kg
Z_{uw}	-56.5	Kg/m	N_{ur}	-8.9	Kg·m/rad
Z_{uq}	-11.8	Kg/rad	N_{uv}	24.9	Kg

where, a_{fin} is the maximum height above the centerline of the vehicle fins. Integrating (48) and (49) over the vehicle axial length, the crossflow added mass are obtained.

$$Y_{\dot{v}} = -\int_{x_t}^{x_f} m_a(x)dx - \int_{x_f}^{x_{f2}} m_{af}(x)dx - \int_{x_{f2}}^{x_{b2}} m_a(x)dx \quad (50)$$

$$Z_{\dot{w}} = Y_{\dot{v}} \quad (51)$$

$$M_{\dot{w}} = \int_{x_t}^{x_f} xm_a(x)dx + \int_{x_f}^{x_{f2}} xm_{af}(x)dx + \int_{x_{f2}}^{x_{b2}} xm_a(x)dx \quad (52)$$

$$N_{\dot{v}} = -M_{\dot{w}} \quad (53)$$

$$Y_{\dot{r}} = N_{\dot{v}} \quad (54)$$

$$Z_{\dot{q}} = M_{\dot{w}} \quad (55)$$

$$M_{\dot{q}} = -\int_{x_t}^{x_f} x^2 m_a(x)dx - \int_{x_f}^{x_{f2}} x^2 m_{af}(x)dx - \int_{x_{f2}}^{x_{b2}} x^2 m_a(x)dx \quad (56)$$

$$N_{\dot{r}} = M_{\dot{q}} \quad (57)$$

Table 16 shows the fin parameters. Table 17 shows the limits of integration. The final crossflow added mass coefficient values are given in Table 18.

3) ROLLING ADDED MASS

To estimate the rolling added mass, the following assumptions will be made.

- The relatively smooth sections of the vehicle hull do not generate any added mass in roll.
- The added mass generated by small protuberances will be neglected.

Given these assumptions, only the hull section containing the vehicle fixed fin is considered. The empirical equation for the added mass of a rolling circle with fins is given in [44] as

$$K_{\dot{p}} = \int_{x_f}^{x_{f2}} \frac{2}{\pi} \rho a^4 dx \quad (58)$$

where a is the fin height above the vehicle centerline. The final value of $K_{\dot{p}}$ is given in Table 18.

B. DAMPING TERMS

The UVMS is a highly coupled and nonlinear system. In order to simplify modeling, the following assumptions will be made.

- Assume the vehicle is symmetric in both horizontal plane ($xy-$plane) and vertical plane ($xz-$plane).
- Any damping terms greater than second-order will be neglected.
- The linear and angular coupled terms will be neglected.

1) AXIAL DRAG

Equation (59) yields the axial drag coefficient.

$$X_{u|u|} = -\frac{1}{2}\rho c_{\text{d}} A_{\text{f}} \quad (59)$$

where ρ is the fluid density. A_f is the frontal area of the vehicle. c_d is the axial drag of the vehicle which can be calculated [45] as

$$c_{\text{d}} = \frac{c_{\text{s}}\pi A_{\text{p}}}{A_{\text{f}}}[1 + 60(\frac{d}{l})^3 + 0.0025(\frac{l}{d})] \quad (60)$$

where $A_p = lp$ is the vehicle plan area. The estimated value of c_s is 3.397×10^{-3} in [45].

2) CROSSFLOW DRAG

The cross flow drag is considered to be the sum of the hull drag and the fin drag. Based on the strip theory, the hull drag is approximated as the sum of the drags on the two-dimensional

cylindrical vehicle cross-sections. This is a rough estimation. It is necessary to adjust the crossflow drag terms based on comparisons with the experimental data. The nonlinear crossflow drag coefficients of the vehicle are represented as follows:

$$Y_{v|v|} = -\frac{1}{2}\rho c_{dc} \int_{x_t}^{x_b} 2R(x)dx - 2(\frac{1}{2}\rho S_{fin}c_{df}) \tag{61}$$

$$Z_{w|w|} = Y_{v|v|} \tag{62}$$

$$M_{w|w|} = -\frac{1}{2}\rho c_{dc} \int_{x_t}^{x_b} 2xR(x)dx - 2x_{fin}(\frac{1}{2}\rho S_{fin}c_{df}) \tag{63}$$

$$N_{v|v|} = -M_{w|w|} \tag{64}$$

$$Y_{r|r|} = -\frac{1}{2}\rho c_{dc} \int_{x_t}^{x_b} 2x|x|R(x)dx + 2x_{fin}|x_{fin}|(\frac{1}{2}\rho S_{fin}c_{df}) \tag{65}$$

$$Z_{q|q|} = -Y_{r|r|} \tag{66}$$

$$M_{q|q|} = -\frac{1}{2}\rho c_{dc} \int_{x_t}^{x_b} 2|x|^3 R(x)dx - 2|x_{fin}|^3 (\frac{1}{2}\rho S_{fin}c_{df}) \tag{67}$$

$$N_{r|r|} = -M_{q|q|} \tag{68}$$

where ρ is the fluid density. $R(x)$ is the hull radius shown in (1-2). c_{dc} is the drag coefficient of a cylinder which is estimated as 1.1 in [45]. c_{df} is the cross flow drag coefficient of the fins which is estimated as 0.56 in [9]. x_{fin} is the axial position of the fin. S_{fin} is the fin planform area.

Table 16 shows the fin parameters. Table 17 shows the limits of integration. The final crossflow drag coefficient values are given in Table 18.

3) ROLLING DRAG

The rolling drag is approximated as the drag of fins, as shown in the following equation.

$$K_{p|p|} = Y_{vvf}r_{mean}^3 \tag{69}$$

where Y_{vvf} is the rolling drag coefficient of the fin. r_{mean} is the mean fin height above the vehicle centerline.

This is a rough approximation for the actual value. It would be better to correct this term based on comparisons with the experimental data. The fin parameters are given in Table 16. The final value of $K_{p|p|}$ is given in Table 18.

C. LIFT

The lift force is considered to be the sum of the hull lift and the fin lift. Based on the empirical formula developed by [46], the lift force coefficients are expressed as follows:

$$Y_{uv} = Z_{uw} = -\frac{1}{2}\rho d^2 c_{lb} - \rho c_{lf}S_{fin} \tag{70}$$

$$Y_{ur} = -Z_{uq} = -\rho c_{lf}S_{fin}x_{fin} \tag{71}$$

where c_{lb} is the body lift coefficient which is expressed as $c_{lb} = (\frac{l}{d})c_{lb}^0(\frac{180}{\pi})$ in [46], where ($c_{lb}^0 = 0.003$, when $6.7 \leq \frac{l}{d} \geq 10$). c_{lf} is the fin lift coefficient.

The lift moment coefficients are expressed as follows:

$$M_{uw} = -N_{uv} = -\frac{1}{2}\rho d^2 c_{lb}x_{cp} + \rho c_{lf}S_{fin}x_{fin} \tag{72}$$

$$M_{uq} = N_{ur} = -\rho c_{lf}S_{fin}x_{fin}^2 \tag{73}$$

where $x_{cp} = -0.65l - x_{zero}$ and $x_{zero} = -x_{cg}$. x_{cg} is the center of gravity with respect to the origin of the vehicle nose. Table 16 shows the fin parameters. The final lift coefficient values are given in Table 18.

APPENDIX B
ITERATIVE FORMULA OF LINEAR AND ANGULAR VELOCITY AND ACCELERATION

The integration algorithm for the revolute joint can be referred to [47].

Outward iterations $k:0 \rightarrow n-1$

$$^{k+1}\omega_{k+1} = R_k^{k+1}(^k\omega_k + z\dot{q}_{k+1}) \tag{74}$$

$$^{k+1}\dot{\omega}_{k+1} = R_k^{k+1}(^k\dot{\omega}_k + ^k\omega_k \times z\dot{q}_{k+1} + z\ddot{q}_{k+1}) \tag{75}$$

$$^{k+1}v_{k+1} = R_k^{k+1}{}^k v_k + {}^{k+1}\omega_{k+1} \times {}^{k+1}d_{k+1/k} \tag{76}$$

$$^{k+1}v_{c,k+1} = R_k^{k+1}{}^k v_k + {}^{k+1}\omega_{k+1} \times {}^{k+1}d_{k/k_c} \tag{77}$$

$$^{k+1}\dot{v}_{k+1} = R_k^{k+1}{}^k \dot{v}_k + {}^{k+1}\dot{\omega}_{k+1} \times {}^{k+1}d_{k+1/k}$$
$$+ {}^{k+1}\omega_{k+1} \times ({}^{k+1}\omega_{k+1} \times {}^{k+1}d_{k+1/k}) \tag{78}$$

where R_k^{k+1} is the rotation matrix that relates frame $\{k\}$ to frame $\{k+1\}$. z is the unit vector along the $z-$axis. q is the generalized joint position. $^k\omega_k$ is the angular velocity of link k. $^k\dot{\omega}_k$ is the angular acceleration of link k. $^k v_k$ is the linear velocity of link k and $^k\dot{v}_k$ is the corresponding time derivative. $^{k+1}v_{c,k+1}$ is the linear velocity of the center of mass of link $k+1$ and $^{k+1}\dot{v}_{c,k+1}$ is the corresponding time derivative. $^{k+1}d_{k+1/k}$ is the position vector from joint $k+1$ to joint k. $^{k+1}d_{k/k_c}$ is the position vector from frame k (joint $k+1$) to the center of mass of link k.

REFERENCES

[1] S. Mcmillan, D. E. Orin, and R. B. McGhee, "Efficient dynamic simulation of an underwater vehicle with a robotic manipulator," *IEEE Trans. Syst., Man, Cybern.*, vol. 25, no. 8, pp. 1194–1206, Aug. 1995.

[2] T. W. Mclain, S. M. Rock, and M. J. Lee, "Experiments in the coordinated control of an underwater arm/vehicle system," *Auto. Robots*, vol. 3, nos. 2–3, pp. 213–232, 1996.

[3] I. Scholberg and T. I. Fossen, "Modelling and control of underwater vehicle-manipulator systems," in *Proc. Conf. Mar. Craft Maneuvering Control*, 1994, pp. 45–57.

[4] T. J. Tarn, G. A. Shoults, and S. P. Yang, "A dynamic model of an underwater vehicle with a robotic manipulator using Kane's method," *Auton. Robot.*, vol. 3, nos. 2–3, pp. 269–283, 1996.

[5] G. Antonelli, *Underwater Robots: Motion and Force Control of Vehicle-Manipulator Systems*, 3rd ed. Berlin, Germany: Springer, 2013, pp. 52–55.

[6] J. Han, J. Park, and W. K. Chung, "Robust coordinated motion control of an underwater vehicle-manipulator system with minimizing restoring moments," *Ocean Eng.*, vol. 38, no. 10, pp. 1197–1206, Jul. 2011.

[7] D. F. Myring, "A theoretical study of body drag in subcritical axisymmetric flow," *Aeronaut. Quart.*, vol. 27, no. 3, pp. 186–194, Aug. 1976.

[8] J. V. N. De Sousa, A. R. L. De Macêdo, W. F. De Amorim Junior, and A. G. B. De Lima, ''Numerical analysis of turbulent fluid flow and drag coefficient for optimizing the AUV hull design,'' *Open J. Fluid Dyn.*, vol. 4, no. 3, pp. 263–277, 2014.

[9] T. Prestero, ''Verification of a six-degree of freedom simulation model for the REMUS autonomous underwater vehicles,'' M.S. thesis, Dept. Ocean Eng. Mech. Eng., MIT, Cambridge, MA, USA, 2001, pp. 25–35.

[10] J. N. Newman, *Marine Hydrodynamics*. Cambridge, MA, USA: MIT Press, 1977.

[11] T. Perez and T. I. Fossen, ''A MATLAB toolbox for parametric identification of radiation-force models of ships and offshore structures,'' *Model., Identificat. Control*, vol. 30, no. 1, pp. 1–15, 2009.

[12] M. S. Triantafyllou, *Maneuvering and Control of Surface and Underwater Vehicles* (Lecture Notes for MIT Ocean Engineering Course), vol. 13. 1996, p. 49.

[13] M. S. Naik and S. N. Singh, ''State-dependent Riccati equation-based robust dive plane control of AUV with control constraints,'' *Ocean Eng.*, vol. 34, nos. 11–12, pp. 1711–1723, Aug. 2007.

[14] M. Dannigan and G. Russell, ''Evaluation and reduction of the dynamic coupling between a manipulator and an underwater vehicle,'' *IEEE J. Ocean. Eng.*, vol. 23, no. 3, pp. 260–273, Jul. 1998.

[15] C. Barbalată, M. W. Dunnigan, and Y. Pétillot, ''Dynamic coupling and control issues for a lightweight underwater vehicle manipulator system,'' in *Proc. Oceans*, 2015, pp. 1–6.

[16] C. Barbalată, M. W. Dunnigan, and Y. Pétillot, ''Reduction of the dynamic coupling in an underwater vehicle-manipulator system using an inverse dynamic model approach,'' *IFAC-PapersOnLine*, vol. 48, no. 2, pp. 44–49, Dec. 2015.

[17] M. Santhakumar, *Investigation Into the Dynamics and Control of an Underwater Vehicle-Manipulator System*. London, U.K.: Hindawi, 2013.

[18] O. Korkmaz, S. K. Ider, and M. K. Ozgoren, ''Trajectory tracking control of an underactuated underwater vehicle redundant manipulator system,'' *Asian J. Control*, vol. 18, no. 5, pp. 1593–1607, Sep. 2016.

[19] Y. Taira, S. Sagara, and M. Oya, ''Model-based motion control for underwater vehicle-manipulator systems with one of the three types of servo subsystems,'' *Artif. Life Robot.*, vol. 25, pp. 133–148, 2020.

[20] H. Mahesh, J. Yuh, and R. Lakshmi, ''A coordinated control of an underwater vehicle and robotic manipulator,'' *J. Robot. Syst.*, vol. 8, no. 3, pp. 339–370, Jun. 1991.

[21] G. Antonelli, F. Caccavale, and S. Chiaverini, ''Adaptive tracking control of underwater vehicle-manipulator systems based on the virtual decomposition approach,'' *IEEE Trans. Robot. Autom.*, vol. 20, no. 3, pp. 594–602, Jun. 2004.

[22] Y. Taira, M. Oya, and S. Sagara, ''Adaptive control of underwater vehicle-manipulator systems using radial basis function networks,'' *Artif. Life Robot.*, vol. 17, no. 1, pp. 123–129, Oct. 2012.

[23] S. Mohan and J. Kim, ''Indirect adaptive control of an autonomous underwater vehicle-manipulator system for underwater manipulation tasks,'' *Ocean Eng.*, vol. 54, pp. 233–243, Nov. 2012.

[24] Y. Dai and S. Yu, ''Design of an indirect adaptive controller for the trajectory tracking of UVMS,'' *Ocean Eng.*, vol. 151, pp. 234–245, Mar. 2018.

[25] Y. Wang, B. Chen, and H. Wu, ''Joint space tracking control of underwater vehicle-manipulator systems using continuous nonsingular fast terminal sliding mode,'' *Proc. Inst. Mech. Eng. M, J. Eng. Maritime Environ.*, vol. 232, no. 4, pp. 448–458, 2018.

[26] H. Han, Y. Wei, and L. Guan, ''Trajectory tracking control of underwater vehicle-manipulator systems using uncertainty and disturbance estimator,'' in *Proc. OCEANS MTS/IEEE*, Charleston, SC, USA, Oct. 2018, pp. 1–6.

[27] B. Xu, S. R. Pandian, and F. Petry, ''A sliding mode fuzzy controller for underwater vehicle-manipulator systems,'' in *Proc. OCEANS MTS/IEEE*, Washington, DC, USA, Jun. 2005, pp. 1–6.

[28] G. Xu, Y. Guo, and X. Xiang, ''Motion control and computer simulation for underwater vehicle-manipulator systems,'' in *Proc. ICMA*, 2007, pp. 1368–1373.

[29] H. Nejatbakhsh Esfahani, V. Azimirad, and M. Danesh, ''A time delay controller included terminal sliding mode and fuzzy gain tuning for underwater vehicle-manipulator systems,'' *Ocean Eng.*, vol. 107, pp. 97–107, Oct. 2015.

[30] W. M. Bessa, M. S. Dutra, and E. Kreuzer, ''Depth control of remotely operated underwater vehicles using an adaptive fuzzy sliding mode controller,'' *Robot. Auto. Syst.*, vol. 56, no. 8, pp. 670–677, Aug. 2008.

[31] G. V. Lakhekar and L. M. Waghmare, ''Robust maneuvering of autonomous underwater vehicle: An adaptive fuzzy PI sliding mode control,'' *Intell. Service Robot.*, vol. 10, no. 3, pp. 195–212, Jul. 2017.

[32] P. S. Londhe and B. M. Patre, ''Adaptive fuzzy sliding mode control for robust trajectory tracking control of an autonomous underwater vehicle,'' *Intel. Serv. Robot.*, vol. 12, no. 1, pp. 87–102, Jan. 2019.

[33] H. Wang, P. X. Liu, X. Zhao, and X. Liu, ''Adaptive fuzzy finite-time control of nonlinear systems with actuator faults,'' *IEEE Trans. Cybern.*, to be published.

[34] H. Wang, W. Liu, J. Qiu, and P. X. Liu, ''Adaptive fuzzy decentralized control for a class of strong interconnected nonlinear systems with unmodeled dynamics,'' *IEEE Trans. Fuzzy Syst.*, vol. 26, no. 2, pp. 836–846, Apr. 2018.

[35] X. Huo, L. Ma, X. Zhao, B. Niu, and G. Zong, ''Observer-based adaptive fuzzy tracking control of MIMO switched nonlinear systems preceded by unknown backlash-like hysteresis,'' *Inf. Sci.*, vol. 490, pp. 369–386, Jul. 2019.

[36] X.-H. Chang, ''Robust nonfragile H_∞ filtering of fuzzy systems with linear fractional parametric uncertainties,'' *IEEE Trans. Fuzzy Syst.*, vol. 20, no. 6, pp. 1001–1011, Dec. 2012.

[37] X. Chang, C. Yang, and J. Xiong, ''Quantized fuzzy output feedback H_∞ control for nonlinear systems with adjustment of dynamic parameters,'' *IEEE Trans. Syst., Man, Cybern., Syst.*, vol. 49, no. 10, pp. 2005–2015, Oct. 2019.

[38] X. Zhao, X. Wang, L. Ma, and G. Zong, ''Fuzzy-approximation-based asymptotic tracking control for a class of uncertain switched nonlinear systems,'' *IEEE Trans. Fuzzy Syst.*, to be published, doi: 10.1109/TFUZZ.2019.2912138.

[39] R. Palm, ''Sliding mode fuzzy control,'' in *Proc. Int. Conf. Fuzzy Syst.*, San Diego, CA, USA, 1992, pp. 519–526.

[40] P. S. Londhe, S. Mohan, and B. M. Patre, ''Robust task-space control of an autonomous underwater vehicle-manipulator system by PID-like fuzzy control scheme with disturbance estimator,'' *Ocean Eng.*, vol. 139, pp. 1–13, Apr. 2017.

[41] P. S. Londhe, M. Santhakumar, and B. M. Patre, ''Task space control of an autonomous underwater vehicle manipulator system by robust single-input fuzzy logic control scheme,'' *IEEE J. Ocean. Eng.*, vol. 42, no. 1, pp. 13–28, May 2016.

[42] Y. Wu, D. Zou, P. Liu, and W. Yu, ''Dynamic magnetometer calibration and alignment to inertial sensors by Kalman filtering,'' *IEEE Trans. Contr. Syst. Technol.*, vol. 26, no. 2, pp. 716–723, Mar. 2018.

[43] G. Salavisidis, A. Munafo, C. Harris, T. Prmapart, R. Templeton, and M. Smart, ''Terrain-aided navigation for long-endurance and deep-rated autonomous underwater vehicles,'' *J. Field Robot.*, vol. 36, pp. 447–474, Mar. 2018.

[44] R. D. Blevins, *Formulas for Natural Frequency and Mode Shape*. Malabar, FL, USA: Krieger Publishing, 1979, p. 407.

[45] S. F. Hoerner, *Fluid Dynamic Drag*. 1965, pp. 3–12.

[46] S. F. Hoerner and H. V. Borst, *Fluid Dynamic Lift*, 2nd ed. 1985, pp. 2–3.

[47] J. J. Craig, *Introduction to Robotics*, 3nd ed. Boston, MA, USA: Addison-Wesley, 1986, p. 176.

HAN HAN received the B.S. degree in automation from the North China University of Water Resources and Electric Power, Zhengzhou, China, in 2013, and the master's degree in instrument science and technology from Harbin Engineering University, Harbin, China, where she is currently pursuing the Ph.D. degree in control science and engineering. Her current research interests include modeling, coordinate control, and disturbance observation for underwater vehicle manipulator systems.

YANHUI WEI received the B.S., M.S., and Ph.D. degrees in mechanical engineering from the Harbin Institute Technology, Harbin, China, in 2001, 2003, and 2008, respectively. From 2008 to 2010, he was a Research Associate with Control Science and Engineering Mobile Station, Harbin Engineering University, Harbin. From 2010 to 2015, he was a Lecturer of precision instrument and machinery with Harbin Engineering University, where he has been an Associate Professor of precision instrument and machinery, since July 2016. His current research interests include reconfigurable modular robots, intelligent control, underwater vehicle systems, and underwater navigation.

XIUFEN YE received the B.S. and M.S. degrees in control theory and control engineering, and the Ph.D. degree in control science and engineering from Harbin Engineering University (formerly known as Harbin Shipbuilding Engineering Institute), Harbin, China, in 1987, 1990, and 2003, respectively. She has been a Professor with the College of Automation, Harbin Engineering University, Harbin, since September 2003. Her current research interests include intelligent underwater vehicles and control systems, digital image processing, object tracking and detection, and sonar images processing and identification.

WENZHI LIU has been a Professorate Senior Engineer of the College of Information and Communication Engineering, Harbin Engineering University, since April 2019. His current research interests include underwater robotics and other new unmanned systems of oceans.

• • •